AD-752 993

STRUCUTRE, PROPERTIES AND RADIATION SENSITIVITY OF ELECTRICALLY BISTABLE MATERIALS. THERMAL STABILITY OF As2Se3-AS2Te3 GLASSES

Derek B. Dove, et al

Florida University

Prepared for:

Advanced Research Projects Agency

6 September 1972

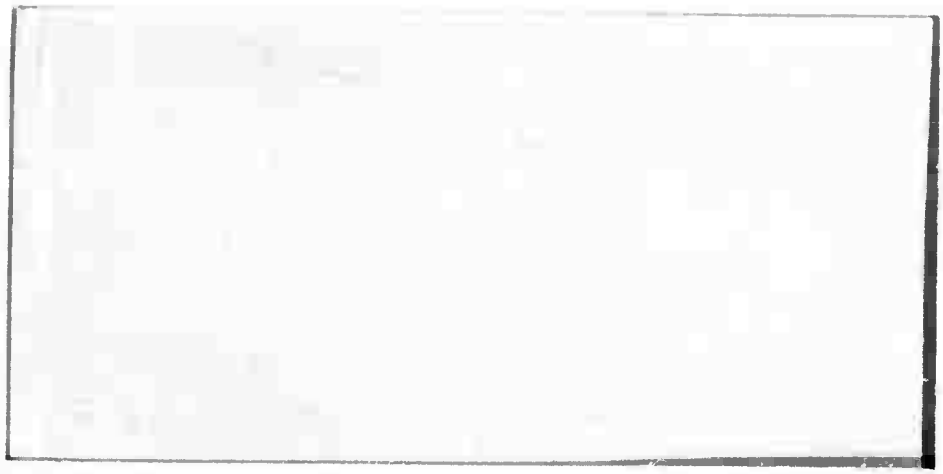

ENGINEERING AND INDUSTRIAL EXPERIMENT STATION

College of Engineering

University of Florida

Gainesville

STRUCTURE, PROPERTIES AND RADIATION SENSITIVITY OF ELECTRICALLY BISTABLE MATERIALS

Technical Report No. 5
6 September 1972

Semiannual Report
(ARPA DAHC04-70-C-0024)

ARPA Order Number:	1562
Program Code Number:	OD10
Name of Contractor:	University of Florida
Effective Date of Contract:	6 February 1970
Contract Expiration Date:	6 Feburary 1973
Amount of Contract:	$140,816
Contract Number:	DAHC04-70-C-0024
Principal Investigator:	Dr. Derek B. Dove, Telephone 904-392-1497
Project Scientist:	Dr. Charles Boghosian, AROD, Telephone 919-286-2285

Sponsored by
Advanced Research Projects Agency
ARPA Order No. DAHC04-70-C-0024

I

Security Classification

DOCUMENT CONTROL DATA - R & D

(Security classification of title, body of abstract and indexing annotation must be entered when the overall report is classified)

1. ORIGINATING ACTIVITY (Corporate author)
University of Florida
Engineering & Industrial Experiment Station
Gainesville, Florida 32601

2a. REPORT SECURITY CLASSIFICATION
Unclassified

2b. GROUP

3. REPORT TITLE
STRUCTURE, PROPERTIES AND RADIATION SENSITIVITY OF ELECTRICALLY BISTABLE MATERIALS

4. DESCRIPTIVE NOTES (Type of report and inclusive dates)
Technical Report, Semiannual, 6 February 1972 to 6 September 1972

5. AUTHOR(S) (First name, middle initial, last name)
Derek B. Dove and Ronald E. Loehman

6. REPORT DATE
6 September 1972

7a. TOTAL NO. OF PAGES
~~86~~ 93

7b. NO. OF REFS

8a. CONTRACT OR GRANT NO.
DAHC04-70-C-0024

b. PROJECT NO.
P-8993-P

c.

d.

9a. ORIGINATOR'S REPORT NUMBER(S)
Technical Report No. 5

9b. OTHER REPORT NO(S) (Any other numbers that may be assigned this report)

10. DISTRIBUTION STATEMENT

11. SUPPLEMENTARY NOTES
This research was supported by Advanced Research Projects Agency

12. SPONSORING MILITARY ACTIVITY
Army Research Office, Durham

13. ABSTRACT

This semiannual report contains some new measurements on the thermal stability of As_2Se_3-As_2Te_3 glasses in which multiple crystallization processes have been found by differential scanning calorimetry. X-ray work is in progress to identify the successive phases formed.

Further discussion is given of the structure of As_2Se_3 films by comparing intensity and rdf curves obtained experimentally with theoretical curves derived from a microcrystallite model. It is found that the nearest neighbor distance and average coordination is the same in the amorphous film and crystalline model. However the third prominent interatomic separation in the crystalline case is absent in the experimental rdf. This strongly indicates that a glassy network model is more in accord with the experimental rdf than a microcrystalline model.

Continuation of the work on the interaction between As_2Se_3 and Cu support grids is strongly indicative of the formation of $Cu_{2-x}Se$ upon heat treatment. Finally a review article on electron diffraction rdfs of amorphous films prepared for the Physics of Thin Films is included.

DD FORM 1 NOV 68 1473

II

Security Classification

14 KEY WORDS	LINK A		LINK B		LINK C	
	ROLE	WT	ROLE	WT	ROLE	WT
Structure of Glasses Thermal Treatment Electron Diffraction Radial Distribution Analysis						

STRUCTURE, PROPERTIES AND RADIATION SENSITIVITY OF ELECTRICALLY BISTABLE MATERIALS

Technical Report No. 5
6 September 1972

Submitted by

D. B. Dove and R. E. Loehman
Department of Materials Science and Engineering
University of Florida
Gainesville, Florida 32601

IV

THERMAL STABILITY OF As_2Se_3-As_2Te_3 GLASSES

Introduction

Interest in the As-Se-Te glass forming system stems from the work of Kolomiets and coworkers[1] who reported extensively on such properties as density, softening temperature, microhardness, viscosity, expansion coefficient, electrical conductivity, thermal emf, dielectric constant and radiation hardness. Switching[2] and semiconducting behavior[1] were demonstrated in a study on $As_2(Se_xTe_{1-x})_3$, however little attention was given to the possibility of phase separation or crystallization.

Bagley and Bair[3] and Bagley and Northover[4] attempted to throw light on the mechanisms of switching for As_2Se_3-As_2Te_3 by differential scanning calorimetry, x-ray diffraction and electron microscopy. Of particular interest were the temperatures, energies and types of thermally induced transformations which occur. For $2As_2Se_3$-As_2Te_3, neither phase separation nor crystallization were observed while As_2Se_3-$3As_2Te_3$ and As_2Se_3-$2As_2Te_3$ were observed to crystallize under the influence of heat treatment without detectable phase separation. All three compositions could be induced to undergo threshold switching while only those glasses which crystallized could be switched into a memory state. They concluded that neither a thermally induced crystallization nor phase separation is required for threshold switching while a memory state can be induced through crystallization.

A recent report by Hill,[5] however, contradicts the results of Bagley and co-workers; Hill found that all bulk glasses he studied for $xAs_2Se_3(1-x)As_2Te_3$ from x = 0 to x = 0.8 are phase separated. Furthermore, DTA experiments revealed two crystallization peaks for some compositions while AC conductivity data showed loss processes which Hill attributed to structural inhomogenities resulting from glass-glass phase separation.

In this report we describe a detailed study of the thermal behavior of glasses in the $As_2(Se_xTe_{1-x})_3$ system carried out to resolve these above noted discrepancies.

Experimental

Bulk glasses were prepared from elemental As, Se and Te in purities of 99.999% or better. Starting materials were sealed in evacuated silica ampoules and reacted in a furnace at 950°C for periods of 24 hours or longer. The ampoules were rapidly quenched from 950°C in an ice-brine mixture. Samples with compositions xAs_2Te_3-$(1-x)As_2Se_3$ and xAs_3Te_2-$(1-x)As_3Se_2$ proved to be amorphous for $0<x<1$ as evidenced by x-ray analysis and conchoidal fracture of the quenched product. Twenty five mg portions of the bulk glasses ground to about 100 mesh were used for the differential scanning calorimetric (DSC) measurements. Scanning rates of from 1.25 to 40 deg/min were used to give the optimum peak response. All measurements were made under a nitrogen atmosphere.

Results and Discussion

Figure 1 shows some of the results of the DSC experiments for As_2Se_3-As_2Te_3. Several features of these experiments are

worth noting. The glass transition temperature shows a smooth increase with increasing selenium concentration over the whole range of compositions. The values obtained are roughly in agreement with the Tg's measured by Bagley and Bair[3] by DSC and with the softening points reported by Kolomiets[1] and by Hill[5]. However, the recent report of Arai and Saito[6] gives a Tg value of 393K for As_2Se_3, a value significantly lower than the Tg of 447K found in this work. The discrepancy possibly is due to the relatively insensitive method for measuring Tg's used by Arai and Saito. Table I lists values of Tg's obtained by different researchers.

A second result from the DSC experiments which is of interest is the multiple peaks observed above the Tg; these are shown in Figure 1. For compositions up to 25 mole precent As_2Se_3 in As_2Te_3, two exothermic transitions were found. X-ray analysis of heat treated samples indicates the exothermic transitions can be attributed to crystallization; however, the spectra obtained are complex and identification of the species crystallizing is a matter under investigation. The two crystallization temperatures show a smooth increase with increasing As_2Se_3 content up to the composition $.33As_2Se_3$-$.67As_2Te_3$ where only one crystallization peak was observed. The fact that the extrapolation of the upper crystallization peak intersects the melting curve shown in Figure 1 at about this composition suggests that the melting point lowering caused by increasing As_2Se_3 is sufficient to prevent crystallization of the second species.

The situation is more complicated at compositions with equimolar or greater concentrations of As_2Se_3. At the equimolar composition the smooth decrease in melting temperature shown in Figure 1 reaches a minimum. Furthermore, another, lower temperature melting peak also makes an appearance at the equimolar composition, indicating a two-stage melting behavior. The two crystallization peaks found for compositions leaner in As_2Se_3 no longer are in evidence. No data were obtained for temperatures greater than Tg for glasses with selenium concentrations greater than $.42As_2Te_3$-$.58As_2Se_3$.

Several different effects occur simultaneously to give the results for the high selenium side of Figure 1 and they greatly complicate the interpretation of the data. A careful examination of the DSC curves indicates that the single melting point shown on the low selenium side of Figure 1 probably is an overlapping double peak which only becomes fully resolved as the two parts are shifted by increasing additions of selenium. For example, the DSC traces for $.92As_2Te_3$-$.08As_2Se_3$ have at most only a slight asymmetry in the endothermic peaks, while for the composition $.67As_2Te_3$-$.33As_2Se_3$ a definite shoulder is found. At the equimolar composition, the two peaks are fully resolved and the temperatures of the onsets of the two transitions are shown in Figure 1.

The shifting and separation of the two exothermic peaks causes them to overlap into the temperature range of the exothermic or crystallization peaks. This complicates the interpretation of the data in that closely spaced exo-and endothermic reactions give DSC traces which resemble S curves which

do not allow the establishment of a base-line. Thus the temperature of the onset of the transition cannot be determined and the absence of exothermic peaks on the right half of Figure 1 most likely is due to a masking effect.

Another complication is the increased volatility of the glasses as selenium content is increased. This primarily has the effect of increasing the noise in the DSC curves. Samples with greater than 58 mole percent As_2Se_3 gave traces which permitted no determination of either crystallization or melting temperatures.

The two-stage crystallization and melting are indicative of some sort of phase separation. As mentioned previously, Bagley and Bair[3] reported results on three of the compositions of our study. For 75/25 and 67/33 As_2Te_3/As_2Se_3 they observed single crystallization peaks while the melting curves were doubly peaked. For the 33/67 glass they observed only the glass transition. Bagley and Northover[4] specifically looked for evidence of phase separation in these compositions as they beam heated thin films in the transmission electron microscope. As with the bulk glasses, crystallization was observed for 75/25 and 67/33 while no crystallization was found for 33/67 As_2Te_3/As_2Se_3. In none of the samples was any evidence of phase separation found. Hill[5] on the other hand, found that all of the bulk glasses $XAs_2Te_3(1-x)As_2Se_3$ from X = 0 to X = .8 are phase separated as evidenced by scanning electron microscope replica techniques. Hill's evidence is suggestive of phase separation, but its usefulness to the question of the switching

mechanism is hampered by the lack of any information on the compositional changes which occur. Furthermore, the lack of agreement between the results of Hill and those of Bagley and co-workers is cause for concern.

The results reported here remain only suggestive until the x-ray work currently in progress is completed. At that time it should be possible to map out in detail the structural and compositional changes which occur as the result of heat treatment for the whole range of compositions in the As_2Se_3-As_2Te_3 system. Furthermore, the kinetics of crystallization are under detailed study for two compositions and the results of this work should be of obvious applicability to models of switching involving thermal transfo mations.

REFERENCES

1. B. T. Kolomiets, phys. stat. sol. 7, 359 (1964).
   B. T. Kolomiets, phys. stat. sol. 7, 713 (1964).

2. J. F. Dewald, A. D. Pearson, W. R. Northover and W. F. Peck, Jr., Electrochem. Soc. Meeting, Los Angeles, May 1962 as reported in ref (19) of B. G. Bagley and H. E. Bair, J. Non-Crystalline Solids, 2, 155 (1970).

3. B. G. Bagley and H. E. Bair, J. Non-Crystalline Solids 2, 155 (1970).

4. B. G. Bagley and W. R. Northover, J. Non-Crystalline Solids 2, 161 (1970).

5. D. J. Hill, M. S. Thesis, Vanderbilt University, May 1972.

6. Kazuo Arai and Shogo Saito,.Jap. J. Appl. Phys., 10, 1669 (1971).

TABLE I

Comparison of Glass Transition Temperatures Obtained by Various Workers.

Composition As_2Te_3/As_2Se_3	Tg°K(This Study)	Tg°K(Kolomiets)[1]	Tg°K(Hill)[5]	Tg°K(Bagley & Bair)[3]
92/8	389			
83/17	391			
80/20			373	
75/25	393	414		
70/30				410
67/33	396		383	
60/40				409
58/42	401	420	398	
55/45				
50/50	406	428		
42/58	409		408	
40/60				
33/67	416		418	
25/75		429		431
20/80		446		
17/83	431			
0/100	447	460	458	

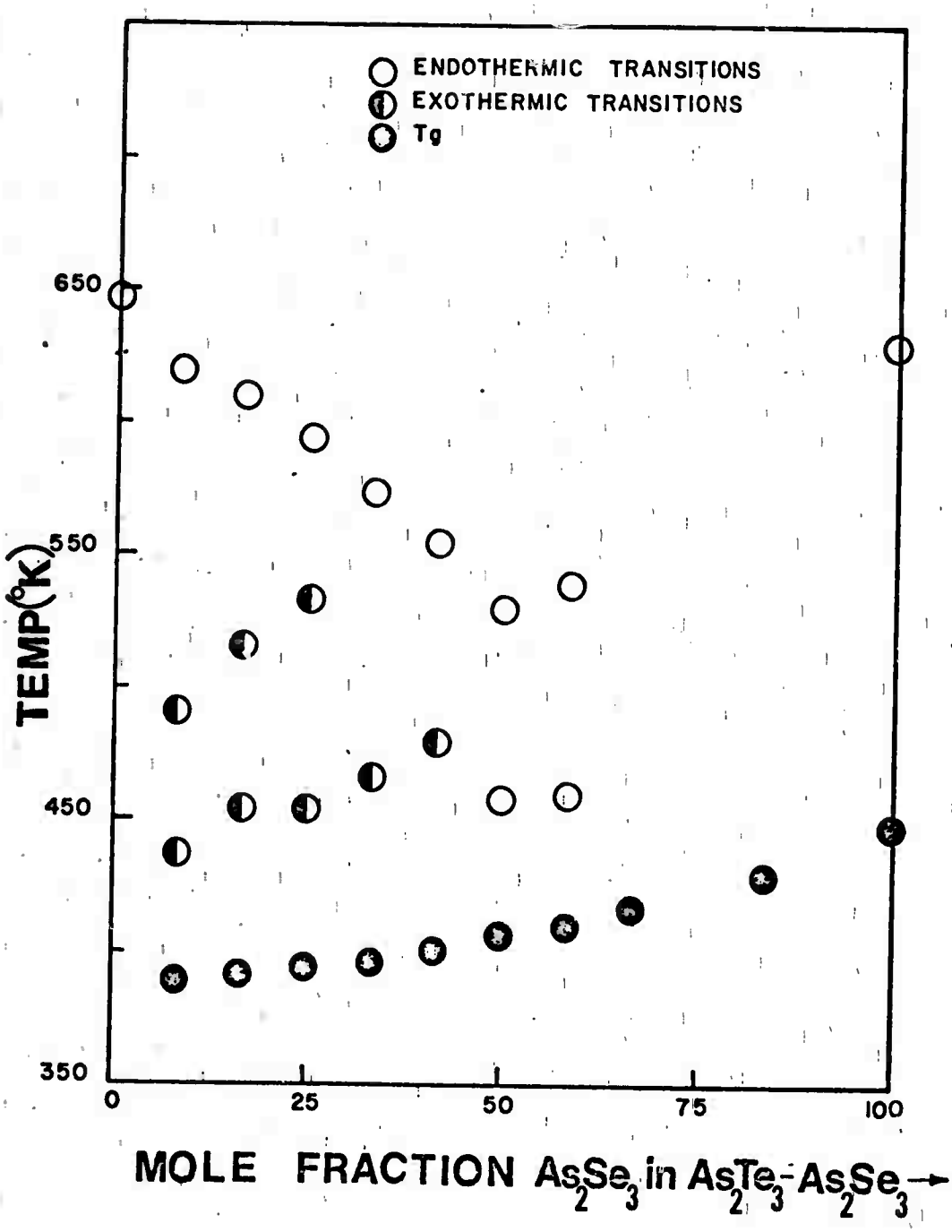

Figure 1. Thermal transitions in As_2Se_3-As_2Te_3 as a function of composition.

STRUCTURE OF As_2Se_3 FILMS

Comparison with Crystalline Material

The observations on As_2Se_3-As_2Te_3 films using direct recording energy filtered electron diffraction were described in a previous report. It was found that the results were consistent with arsenic and selenium or tellurium possessing 3 and 2 neighbors respectively. The nearest neighbor bond lengths were consistent with the sum of covalent atomic radii, but it was not possible to distinguish whether or not chemical ordering exists. In this report further discussion is given of the local order in these glasses, particularly As_2Se_3.

A common feature of the diffuse scattering profiles is the occurance of a peak fairly close to the main beam. Vaipolin and Porai-Koshits[1] have suggested that this peak is due to diffraction from a layer structure since such a structure is characteristic of crystalline As_2Se_3. The only crystalline data for As_2Se_3 is that of Vaipolin[2] indicating an orpiment layer structure, the cell height being equal to the thickness of two layers, and the average coordination numbers for As and Se are close to 3 and 2. The radial distribution functions are therefore consistent with both a glassy randomly bonded net and with a local order similar to that in the crystalline form.

In order to make a more detailed comparison between the glassy and crystalline structures the interference function $s(i(s)-1)$ has been calculated for an array of As_2Se_3 crystallites. The crystallites were taken to consist of 27 unit cells and were

assumed to be randomly oriented. Interatomic distances within a crystallite were calculated by computer and the interference function was generated from

$$s(i(s)-1) = \sum_n \frac{N_n}{2\pi} \sin(2\pi\, r_n\, s)\, \exp(-\alpha_n\, s^2)$$

where N_n = atomic coordination number corresponding to interatomic distance r_n. In the usual notation, $s = 2 \sin \theta/\lambda$. The effect of thermal vibrations is included in the exponential term.

Figure 1 shows a comparison between the calculated interference curve a for the As_2Se_3 crystalline layer structure (with α_n taken to be constant and equal to 0.75) and curve c, the experimental result for the amorphous films.
It can be noted that a small peak is reproduced at a moderately small s value (s = 0.25) as expected. This does not coincide however with the experimental location of the first peak in curve c. The next two major peaks are reproduced reasonably well, while the next crystalline peak is not present at all in the experimental curve. The two curves therefore show similarities and disimilarities and it is not useful to pursue the comparison further. Radial distribution curves were calculated from the interference functions using the numerical Fourier transform carried out over the same range in s values for each curve. The dashed line in Figure 2 shows the result for the amorphous film and the full line shows the rdf obtained for the (theoretical) crystalline case. The expected close correspondence between the nearest neighbor peaks of the two curves

can be noted. The second and third peaks differ appreciably however, the major difference between the curves being the absence of the third (crystalline) peak in the amorphous film case. This would seem to rule out at least the possibility that the film actually consisted of small As_2Se_3 crystallites.

Previous experience has shown that an approximation to the rdf of the amorphous material can be obtained by assuming that interatomic distances in the material are distributed about some mean value with a gaussian distribution whose width increased with value of atomic separation and whose width, for distances greater than the nearest neighbor distance, was considerably greater than the spread due to thermal vibrations. Curve b of Figure 1 shows the interference function calculated in this way with α_n varying from 0.45 to 2.0 at 6Å. This procedure yields a curve intermediate to the theoretical crystalline case and experimental amorphous case. The full and broken lines of Figure 3 show the rdfs calculated from curves b and c respectively of Figure 1. It can be seen that the introduction of increasing disorder in the larger interatomic distances tends to suppress the third peak in the rdf while the first and second peaks are unchanged.

From the above considerations it would appear that the rdf obtained for amorphous As_2Se_3 films is not in detailed agreement with a microcrystalline model but that the nearest neighbor order is essentially the same in the amorphous and crystalline case.

Interaction with Copper

So far crystalline patterns have only been obtained from As_2Se_3 films heat treated on copper grids. Heat treatment on Al or Mo covered grids failed to produce any crystallization at all although As_2Te_3 films can be readily crystallized in this way, giving a ring pattern agreeing in detail with that expected for crystalline As_2Te_3. As noted previously heat treatment on copper grids produced big changes in the intensity distribution and leads to crystallization. Figure 4a shows an intensity profile taken across the ring pattern resulting from heat treating As_2Se_3 film supported on copper screening. Figure 4b shows a selenium film similarly treated. The Table shows the measured d and I/Io values for curve b and the ASTM card values for crystalline $Cu_{2-x}Se$. In the present units, d = 1/s Angstroms. It is apparent that the selenium film formed $Cu_{2-x}Se$ upon crystallization on Cu grids. The curve a from the heated As_2Se_3 films shows that the peaks correspond to peaks occuring in $Cu_{2-x}Se$ but that many of the peaks corresponding to this compound are missing. It is not known at this stage whether the absence of these peaks indicates a prefered orientation of crystallites in the film, or whether this is an effect due to the presence of arsenic.

It is instructive to compare the rdf calculated from the curve 4a with the rdf of as deposited As_2Se_3 films, as shown by the full and broken lines respectively in Figure 5.

The two rdfs appear to differ quite significantly. The nearest neighbor peak of the film heat treated on the copper

grid has shifted to 2.52Å, and the other peak positions are widely separated from the as deposited film curve. Typical bond lengths for As, Se and Cu with Cu are 2.518, 2.438 and 2.556Å respectively. The radial distribution curve is therefore in agreement with the apparent occurance of alloying between As_2Se_3 and Cu.

REFERENCES

1. A. A. Vaipolin and F. A. Porai-Koshits; Soviet Phys. Solid State, Vol. 5, No. 2, p. 497-500 (August, 1963).

2. A. A. Vaipolin; Soviet Phys.-Crystallography, Vol. 10, No. 5, p. 509-512 (March-April, 1966).

TABLE I

Experiment Curve (Se film crystallized on Cu screen)		ASTM Card $Cu_{2-x}Se$	
d, Å	I/Io	d	I/Io
6.137	17%	3.52	5%
3.398	100	3.33	90
2.918	23	2.88	10
2.046	84	2.02	100
1.757	47	1.729	80
1.66	22		
1.434	19	1.434	30
1.3118	19	1.317	20
1.168	26	1.171	40
1.10	14	1.105	20
1.013	10	1.014	10
0.965	11	0.969	10
0.904	9	0.908	20

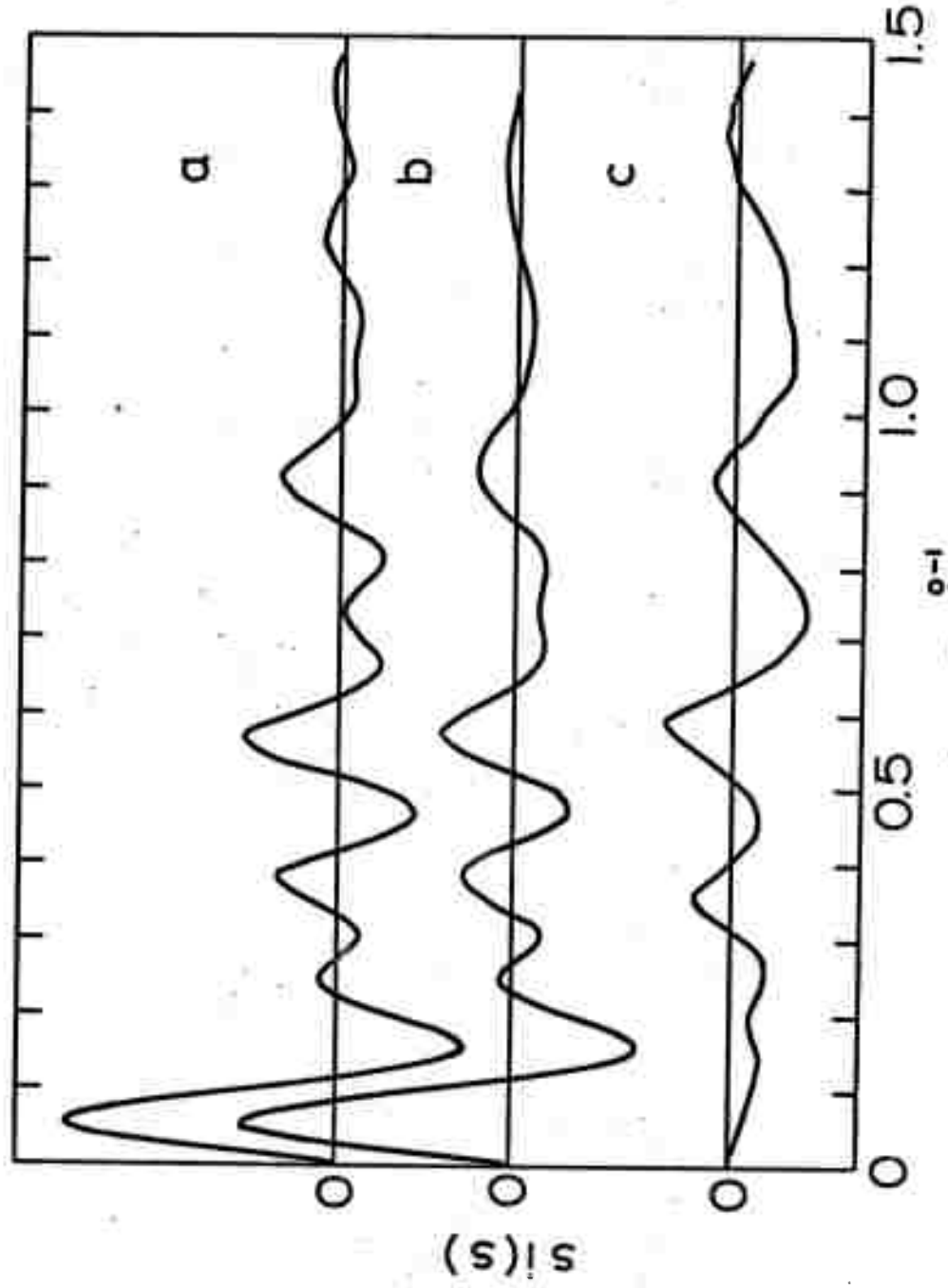

Figure 1. s[i(s)-1] of As_2Se_3

a. Calculated crystalline layer model.

b. Calaulated layer model with varied distribution factors.

c. Normalized amorphous As_2Se_3 intensity curve.

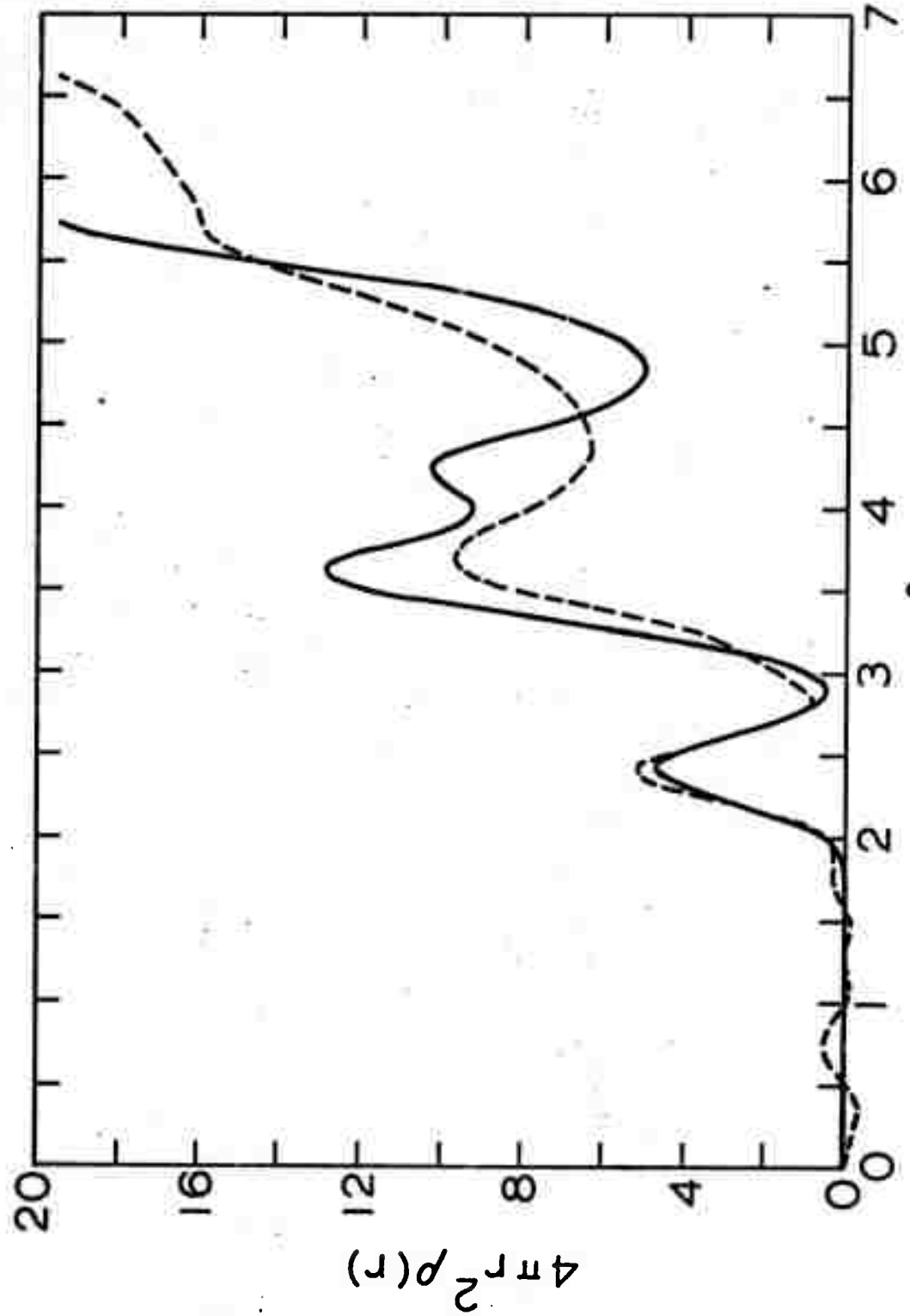

Figure 2. rdf of calculated crystalline layer model of As_2Se_3 (full line)

Experimental rdf of amorphous As_2Se_3 (broken line)

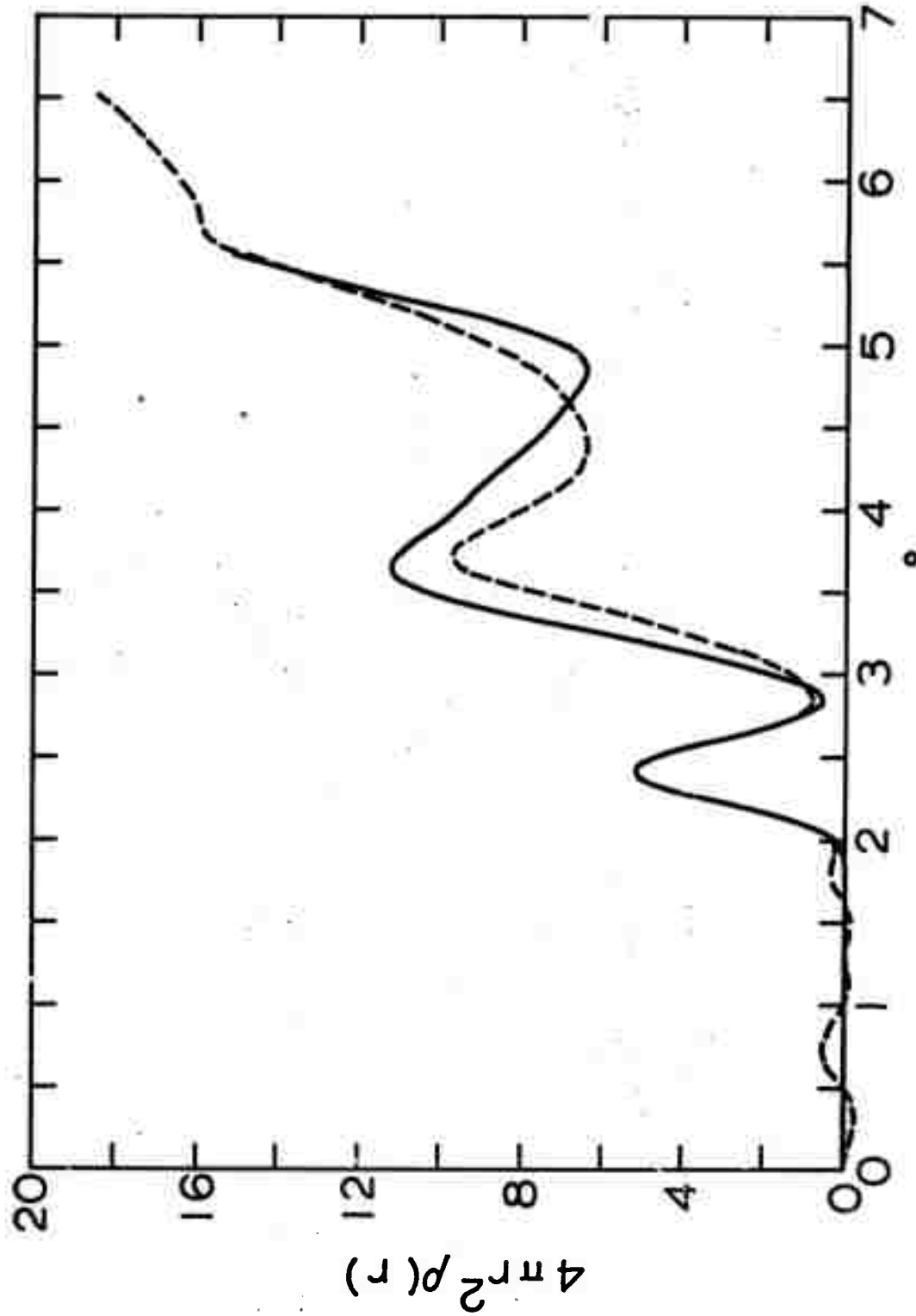

Figure 3. rdf of calculated layer model of As_2Se_3 with varied artificial thermal factor (full line)

rdf of amorphous As_2Se_3 (broken line)

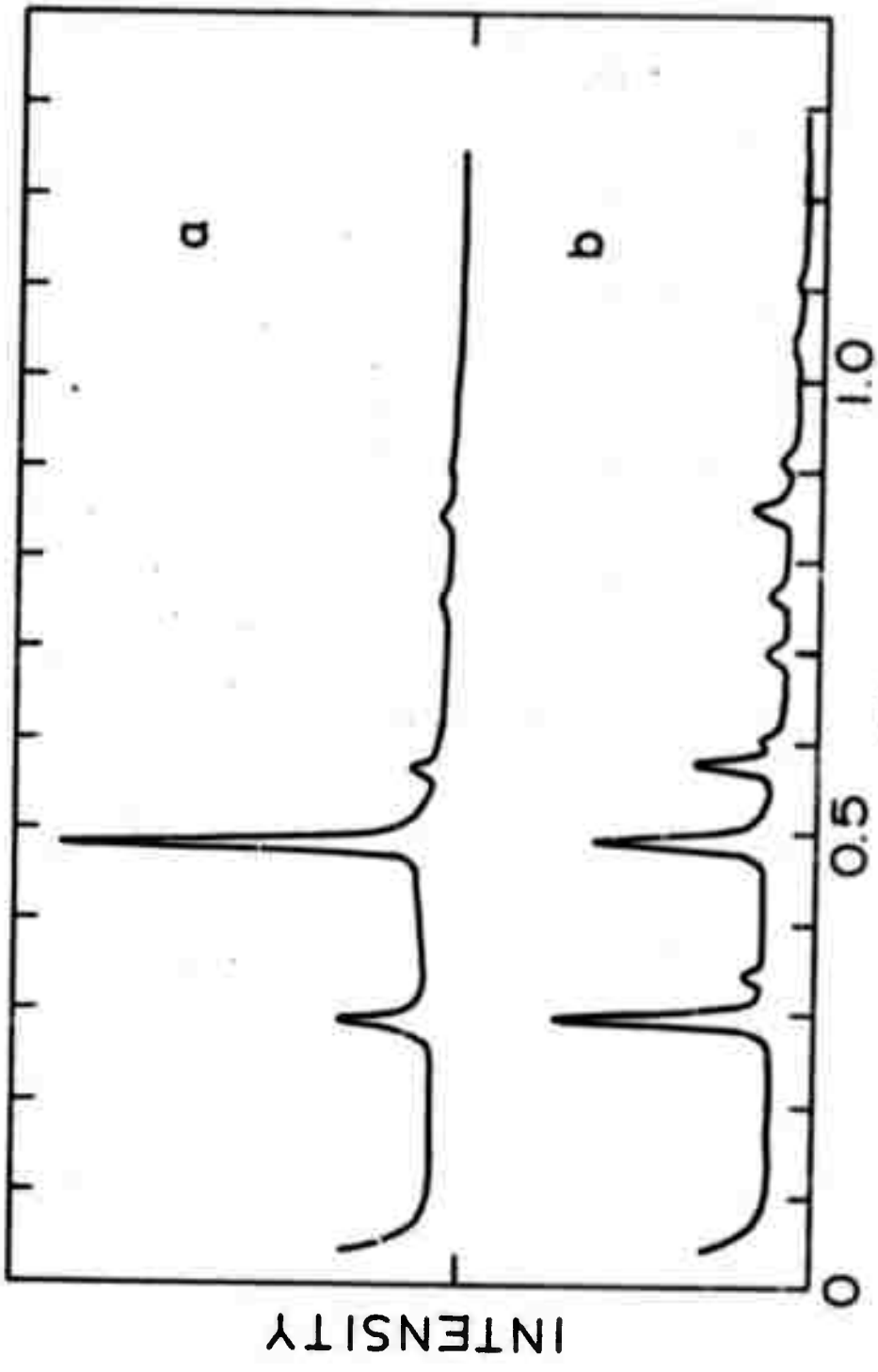

Figure 4. Intensity profiles across electron diffraction patterns of:

a. As_2Se_3 heat treated on Cu mesh.

b. Se heat treated on Cu mesh.

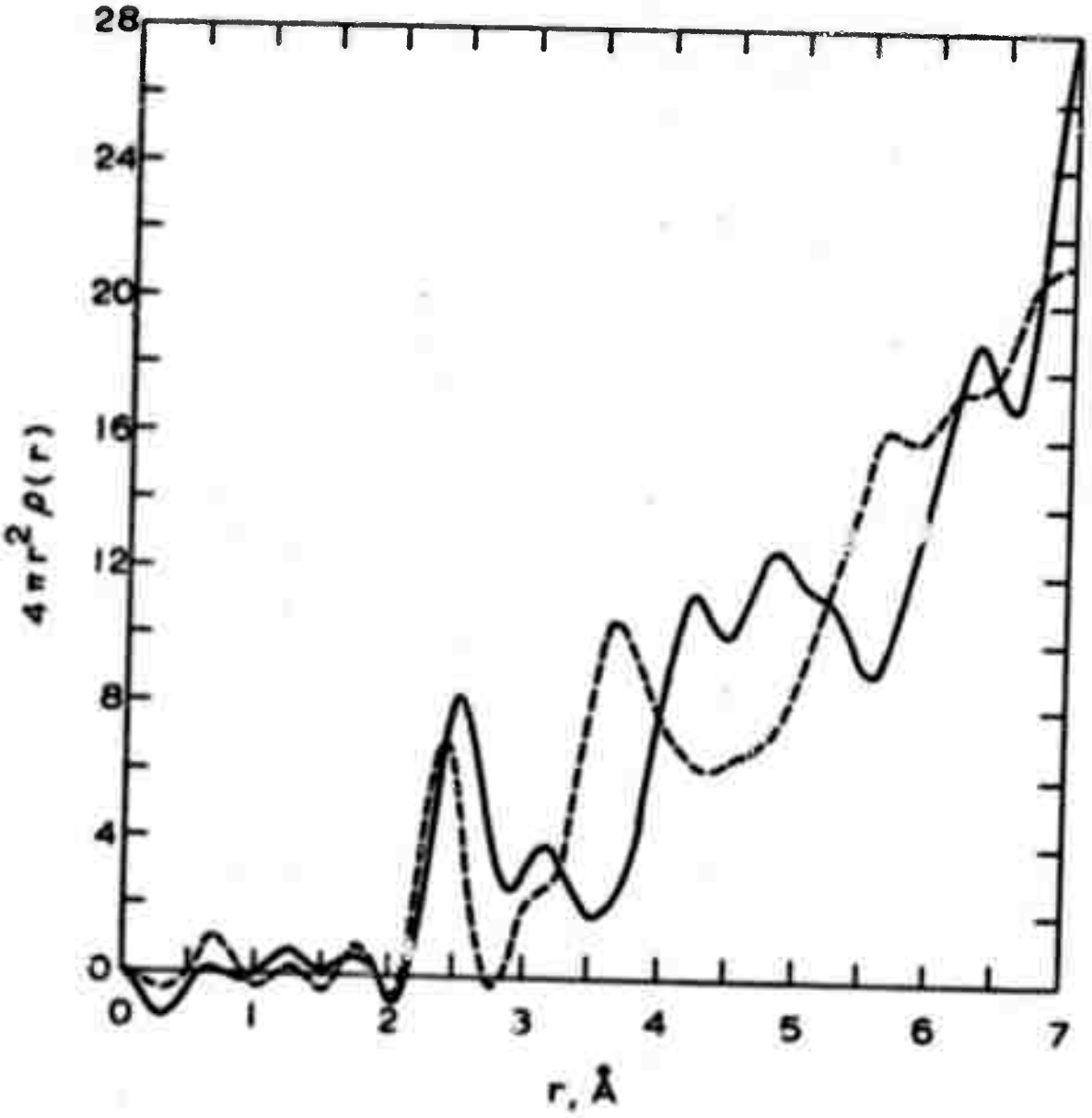

Figure 5. rdf of As_2Se_3 heat treated on Cu mesh (full line)
rdf of Se heat treated on Cu mesh (broken line)

ELECTRON DIFFRACTION ANALYSIS OF THE LOCAL ATOMIC ORDER IN AMORPHOUS FILMS

By

D. B. Dove

Department of Materials Science and Engineering

University of Florida, Gainesville, Florida 32601

A review article prepared for the Physics of Thin Films.

This research was supported by the National Science Foundation and ARO-Durham DAHC04-70-C-0024.

TABLE OF CONTENTS

I. INTRODUCTION

It has been known for many years that thin layers prepared under certain conditions may give extremely diffuse electron or x-ray diffraction patterns that may not be readily interpreted in terms of Bragg diffraction peaks. In the 1930's Germer (1) obtained diffuse patterns from a variety of very thin films during the initial stage of deposition from the vapor. Maxwell and Mosely, on the other hand, examined films of silica thinned from the bulk by a blowing technique (2) and found that the films gave diffuse electron diffraction patterns which could be compared with the x-ray work of Warren et al. (3) on bulk silica.

In more recent years considerable attention has been given to the preparation of a wide variety of materials in thin film form (4,5). In particular, thin film techniques have permitted the preparation of amorphous layers of elements and compounds that have hardly or not at all been obtainable in this form by quenching from the melt. The term amorphous is taken, in the present discussion, to indicate a material in which the atomic arrangement fails to exhibit spatial periodicity. The term is descriptive rather than definitive and attempts at a literal interpretation are to be avoided.

It is to be recognized that diffuse diffraction patterns may arise from several distinctly different types of films that may be conveniently classified as follows:

i) Very finely polycrystalline films, with grain size of order one or two unit cells, yield an extremely diffuse diffraction pattern. Diffusely diffracting

extremely thin films of metals frequently (but not always) fall into this category.

ii) Homogeneous structures such as, for example, some simple glasses in which the statistic degree of order does not vary appreciably from location to location.

iii) Heterogeneous systems, which may, for example, consist of a mixture of immiscible glasses or of small ordered regions in an otherwise homogeneous matrix.

Radial distribution analysis of the diffuse diffraction patterns permits only a statistical characterization, averaged over the sample, in terms of distances between atoms and coordination numbers. Evidence of macroscopic homogeneity or heterogeneity must be obtained by other techniques such as electron microscopy or small angle scattering, and models for the local configurational order in general require confirmation from additional experimentation such as infrared absorption or x-ray absorption edge fine structure.

Finely polycrystalline films as in the first category above are conventionally not regarded as amorphous, although the distinction is not always easily drawn since in such cases grain boundary disorder may constitute a considerable proportion of the whole. The diffuse diffraction patterns from films of this type are among those most amenable to radial distribution analysis.

The absence of distinct structural periodicity in amorphous materials does not exclude the existence of characteristic atomic configurations in which groups of atoms preserve a particular

type of bonding. The character and extent of local configurational ordering may depend on the type of atoms, material preparation and thermal or other treatments. Very typically, strong directional bonding, low substrate temperatures, and system complexity favor the formation of amorphous films.

The analysis of such structures using electron or x-ray diffraction techniques stems directly from the classic work of Debye (6), Zernike and Prins (7) and Debye and Menke (8). The theory is well established and is treated in a number of texts (9,10,11), although certain peculiarities of the technique are seldom made clear in the thin film literature.

The aim of this review is to discuss the theory and technique of the analysis of local atomic configurational order from electron diffraction data and to describe diffraction measurements reported for a wide variety of amorphous films.

Attention is drawn to the valuable information contained in the reviews by Gingrich (12) and Furukawa (13) on the analysis of liquids, by Grigorovici (14) on the structure of amorphous semiconductors, and to a number of conference proceedings (15,16).

II. DIFFRACTION THEORY

1. The Debye Equation

Details of the theory of scattering by amorphous materials may be found in several excellent texts, for example by Hosemann and Bagghi (9), Guinier (10), and Warren (11). The present discussion follows a particularly useful treatment by Pings and

Waser (17). The aim of the diffraction analysis is to determine the radial distribution functions $4\pi r^2\rho_{ij}(r)$, giving the numbers of atoms of type j at distance r from an average atom of type i. The extent to which this may be accomplished in practice is discussed in later sections.

Consider a beam of electrons or x-rays parallel to a vector $\underline{S}_o$, being scattered by an array of N atoms located at positions $\underline{R}_1$, $\underline{R}_2$, $\underline{R}_n$, relative to some origin and having atomic scattering factors f_1, f_2, f_n. Simple geometric-optic arguments show that the intensity scattered in a direction parallel to a new vector $\underline{S}$ is given by

$$I = \sum_{j=1}^{N} f_j^2 + \sum_{\substack{p=1 \\ p\neq q}}^{N} \sum_{q=1}^{N} f_p f_q \exp(2\pi i\, \underline{s}\cdot\underline{r}_{pq}) \qquad (1)$$

where $\underline{s} = (\underline{S}-\underline{S}_o)/\lambda$, $\underline{r}_{pq} = \underline{R}_p - \underline{R}_q$, and λ is the wavelength of the incident and scattered radiation. This is a quite general result for any atomic arrangement, periodic or otherwise. In the case of a crystalline material, $\underline{r}_{pq}$ takes a very specific set of values and sharp diffraction peaks result. The major step in applying this general relation to amorphous materials lies in assuming that for any particular interatomic separation $|\underline{r}_{pq}|$ the direction of $\underline{r}_{pq}$ may take any orientation relative to $\underline{S}_o$ with equal probability. Equation (1) may then be averaged over all orientations to give the Debye equation

$$I = \sum_{j=1}^{N} f_j^2 + \sum_{\substack{p=1 \\ p\neq q}}^{N} \sum_{q=1}^{N} f_p f_q \frac{\sin 2\pi s r_{pq}}{2\pi s r_{pq}} \qquad (2)$$

where $r_{pq} = |\underline{r}_{pq}|$, $s = |\underline{s}| = 2\sin\theta/\lambda$ and 2θ is the angle of deflection of the beam. It is to be noted that in some papers s is taken to be equal to $4\pi\sin\theta/\lambda$. More commonly, in x-ray work, a separate symbol k is used to denote this quantity.

In practice the amorphous material to be investigated may contain only a few different types of atom, but N the total number of atoms illuminated by the beam will be very large. The summation may then be replaced by integration over radial distribution functions $4\pi r^2\rho_{ij}(r)$, representing the number of j type atoms surrounding an i type atom at distance r. Let $x_1, x_2, \ldots x_n$ be the atomic fraction of atoms with scattering factors $f_1, f_2, \ldots f_n$, then

$$I(s) = N \sum_{j=1}^{n} x_j f_j^2 + N \sum_{i=1}^{n} \sum_{j=1}^{n} x_i f_i f_j \int_0^\infty 4\pi r^2 \rho_{ij}(r) \frac{\sin 2\pi sr}{2\pi sr} \sigma(r)dr \quad (3)$$

The $\sigma(r)$ function is introduced to allow for the finite size of scattering volume; i.e., $\sigma(r) \to 0$ as the dimensions of the scattering region are exceeded. The actual form of $\sigma(r)$ depends on the macroscopic shape of the scattering volume. Finally, it must be noted that the atomic density distribution functions $\rho_{ij}(r)$ consist of fluctuations $\rho_{ij}(r)-\bar{\rho}_{ij}$, about a constant mean density of j type atoms $\bar{\rho}_{ij}$. We may therefore make the substitution $\rho_{ij}(r)-\bar{\rho}_{ij}+\bar{\rho}_{ij}$ for $\rho_{ij}(r)$, and obtain

$$I(s) = N \sum_{j=1}^{n} x_j f_j^2$$

$$+ N \sum_{i=1}^{n} \sum_{j=1}^{n} x_i f_i f_j \int_o^\infty 4\pi r^2 [\rho_{ij}(r) - \bar{\rho}_{ij}] \frac{\sin 2\pi sr}{2\pi sr} \sigma(r) dr$$

$$+ N \sum_{i=1}^{n} \sum_{j=1}^{n} x_i f_i f_j \int_o^\infty 4\pi r^2 \bar{\rho}_{ij} \frac{\sin 2\pi sr}{2\pi sr} \sigma(r) dr \qquad (4)$$

The final term gives rise only to a very small angle contribution and this is determined by the macroscopic shape of the illuminated region of the specimen; this contribution is, however, usually unobservable since it is lost in the edge of the undeflected beam. Measurable contributions in the small angle region may arise, however, from voids, precipitates or other significant local density fluctuations, effects not included in the above equation. The small angle terms may therefore be discarded, and hence

$$I(s) = N \sum_{j=1}^{n} x_j f_j^2 + N \sum_{i=1}^{n} \sum_{j=1}^{n} x_i f_i f_j$$

$$\int_o^\infty 4\pi r^2 [\rho_{ij}(r) - \bar{\rho}_{ij}] \frac{\sin 2\pi sr}{2\pi sr} \sigma(r) dr \qquad (5)$$

Finally, for non-crystalline materials $\rho_{ij}(r) - \bar{\rho}_{ij}$ tends to zero with r rapidly compared with the specimen dimensions and $\sigma(r)$ may then be taken equal to unity.

Several special cases may now be discussed; for a one-component, i.e., elemental, material, equation (5) reduces to

$$I(s) = Nf^2(s) + Nf^2(s) \int_o^\infty 4\pi r^2 [\rho(r) - \rho_o] \frac{\sin 2\pi sr}{2\pi sr} dr \qquad (6)$$

while for a binary compound

$$I(s) = N(x_1 f_1^2 + x_2 f_2^2)$$
$$+ Nx_1 f_1^2 \int_o^\infty 4\pi r^2 [\rho_{11}(r) - \bar{\rho}_{11}] \frac{\sin 2\pi sr}{2\pi sr} dr$$
$$+ Nx_1 f_1 f_2 \int_o^\infty 4\pi r^2 [\rho_{12}(r) - \bar{\rho}_{12}] \frac{\sin 2\pi sr}{2\pi sr} dr$$
$$+ Nx_2 f_2 f_1 \int_o^\infty 4\pi r^2 [\rho_{21}(r) - \bar{\rho}_{21}] \frac{\sin 2\pi sr}{2\pi sr} dr$$
$$+ Nx_2 f_2^2 \int_o^\infty 4\pi r^2 [\rho_{22}(r) - \bar{\rho}_{22}] \frac{\sin 2\pi sr}{2\pi sr} dr \qquad (7)$$

2. Calculation of the Radial Distribution Functions

a. Elements. The equation (6) may be rearranged to give

$$s\left[\frac{I(s)}{Nf^2(s)} - 1\right] = 2 \int_o^\infty r[\rho(r) - \rho_o] \sin 2\pi sr dr$$

or $$si(s) = \int_{-\infty}^\infty r[\rho(r) - \rho_o] \sin 2\pi sr dr \qquad (8)$$

where si(s) has been written for the expression on the left-hand side. This is a very remarkable result, being in the form of a Fourier transform, and hence by the inversion property of the transform, the function $r[\rho(r) - \rho_o]$ may be obtained directly (18),

$$r[\rho(r) - \rho_o] = \int_{-\infty}^\infty si(s) \sin 2\pi rs ds \qquad (9)$$

or finally,

$$4\pi r^2 \rho(r) = 4\pi r^2 \rho_o + 8\pi r \int_o^\infty si(s) \sin 2\pi rs ds \qquad (10)$$

Unfortunately, the upper limit of infinity cannot be realized since

i) the intensity falls off rapidly with angle and can only be measured to higher and higher angles at the expense of increasingly unfavorable signal to noise ratio, and

ii) the scattering parameter $s = 2(\sin\theta)/\lambda$ has a maximum value of $2/\lambda$. This is not a limitation in high energy electron diffraction work where the wavelength is extremely small (e.g., $\lambda = 0.06$ Å for a beam energy of 40 keV) but must be considered in the x-ray case.

In practice, the integration is carried out up to a finite limit equal to s_{max}, and termination ripples are generated in the resulting transform. In order to minimize such ripples, si(s) is frequently multiplied by a "terminating" function that decreases monotonically from a value equal to unity at $s = 0$ to a value typically 0.1 at s_{max}. A convenient function is of the form $\exp(-as^2)$. Atomic thermal vibrations are also expected to give rise to a similar damping of the si(s) function.

It is necessary therefore to consider the transform of $g(s)si(s)$ where $g(s)$ is a termination function as described above but in addition has the value zero for $s > s_{max}$. Then

$$\int_0^{s_{max}} g(s)si(s) \sin 2\pi rsds = \int_0^{\infty} g(s)si(s) \sin 2\pi rsds \quad (11)$$

The integral may be evaluated in a very convenient form by employing the Fourier convolution product relationship. This states that the transform of the product of two functions is equal to

convolution products of the transforms of the functions. The (one-dimensional) convolution product of two functions $X_1(x)$ $X_2(x)$ is simply $Y(x) = \int_{-\infty}^{\infty} X_1(u)\, X_2(x-u)du$. Let us denote the cosine transform of the (even) function $g(s)$ by $h(r)$; the sine transform of $si(s)$ has already been given as $r[\rho(r)-\rho_o]$. Now employing the convolution product relationship,

$$\int_0^{\infty} g(s)si(s) \sin 2\pi rsds = 1/2 \int_{-\infty}^{\infty} h(t)(r-t)[\rho(r-t)-\rho_o]dt \qquad (12)$$

This illustrates a very general and important result; the Fourier transform of the $si(s)g(s)$ function (derived from the diffraction data) does not give the radial distribution function directly. Instead, the rdf is convoluted with the transform of the function $g(s)$. In the ideal limiting case of $g(s)$ being unity everywhere, then the transform becomes a delta function and the convolution product becomes simply $r[\rho(r)-\rho_o]$, from which the rdf $4\pi r^2\rho(r)$ may be calculated. Figure 1 illustrates the significance of this effect for an array of isolated, randomly oriented, cells of the diamond structure, with a small atomic thermal vibration. The transform of the calculated $si(s)$ function taken over infinite range is shown in Fig. 1a. However, experimental circumstances frequently limit s_{max} to a value of order 2 to 3. The transform over the range $s_{max} = 1.95$ taking $g(s) = 1.0$ over this range is shown in Fig. 1b. The transform taking $g(s)$ to be a gaussian function falling to a value 0.1 at s_{max} is shown in Fig. 1c. Two major effects are to be noted.

i) The finite range transform of $si(s)$ does not directly give the required distribution $r[\rho(r)-\rho_o]$

of the material, but peaks are broadened and changed in shape to a greater or lesser extent.

ii) Small "ripple" peaks exist to either side of the main peak which depend on the form of the g(s) function. Such ripples are frequently regarded as spurious and are eliminated from the transform by employing a gaussian termination function or other means, at the expense of an increase in peak widths.

b. Binary Compounds. The analysis of compounds is complicated by two factors, notably by the necessity of determining several density functions ρ_{11}, ρ_{12}, etc., and by the mixed products of scattering factors that cannot be factored away from the right-hand side of equation (7). The essential feature of taking the Fourier transform still applies, however, and equation (7) may be rearranged to give

$$si(s) = \frac{f_1^2}{F^2} si_{11}(s) + \frac{f_1 f_2}{F^2} si_{12}(s) + \frac{f_2 f_1}{F^2} si_{21}(s) + \frac{f_2^2}{F^2} si_{22}(s) \qquad (13)$$

where $$si(s) = s[I(s) - N(x_1 f_1^2 + x_2 f_2^2)]/NF^2 \qquad (14)$$

and $$si_{pq}(s) = \int_{-\infty}^{\infty} x_p r[\rho_{pq}(r) - \bar{\rho}_{pq}] \sin 2\pi rsds \qquad (15)$$

$F^2(s)$ is some normalizing function, typically, but not necessarily, equal to $(x_1f_1+x_2f_2)^2$. We may now evaluate the transform of $g(s)si(s)$ where $g(s)$ is a terminating and truncating function as before. Then by the convolution product theorem,

$$2\int_o^\infty g(s)si(s)\sin 2\pi rsds = x_1\int_{-\infty}^{\infty}Q_{11}(t)(r-t)[\rho_{11}(r-t)-\bar{\rho}_{11}]dt$$
$$+ x_1\int_{-\infty}^{\infty}Q_{12}(t)(r-t)[\rho_{12}(r-t)-\bar{\rho}_{12}]dt$$
$$+ x_2\int_{-\infty}^{\infty}Q_{21}(t)(r-t)[\rho_{21}(r-t)-\bar{\rho}_{21}]dt$$
$$+ x_2\int_{-\infty}^{\infty}Q_{22}(t)(r-t)[\rho_{22}(r-t)-\bar{\rho}_{22}]dt \qquad (16)$$

where $Q_{pq}(t) = \int_{-\infty}^{\infty} g(t)\,\frac{f_1f_2}{F^2}\cos 2\pi rsds.$

Making use of the relations $\bar{\rho}_{pq} = x_q\rho_o$ and noticing that the area under the Q_{ij} functions is just equal to $g(o)f_i(o)f_j(o)/F^2(o)$, then,

$$\int_o^\infty g(s)si(s)\sin 2\pi rsds = x_1\int_{-\infty}^{\infty}Q_{11}(t)(r-t)\,\rho_{11}(r-t)dt$$
$$+ x_1\int_{-\infty}^{\infty}Q_{12}(t)(r-t)\,\rho_{12}(r-t)dt$$
$$+ x_2\int_{-\infty}^{\infty}Q_{21}(t)(r-t)\,\rho_{21}(r-t)dt$$
$$+ x_2\int_{-\infty}^{\infty}Q_{22}(t)(r-t)\,\rho_{22}(r-t)dt$$
$$- r\rho_o g(o)[x_1f_1(o)+x_2f_2(o)]^2/F^2(o) \qquad (17)$$

The general result may be noted; the transform of the data yields a curve which consists of the required distribution functions

convoluted with functions whose form depends on the atomic scattering factors and on g(s).

A major fundamental problem thus arises in the case of materials containing more than one kind of atomic species. One diffraction experiment is not sufficient to determine the individual ρ_{ij} functions even though the Q_{ij} functions can be readily calculated. Keating (19) has given a discussion of this problem and has pointed out the possibility that the individual ρ_{ij} functions may be determined by carrying out diffraction experiments using different types of radiation, e.g., X-rays, electrons and neutrons.

It is to be noted that peaks in the distribution functions are broadened and that ripple peaks may exist in the computed transform. In addition, the areas of peaks in the radial distributions $4\pi r^2\rho_{ij}(r)$ are weighted by factors $g(o)f_i(o)f_j(o)/F^2(o)$.

c. Microcrystalline Films. When the grain size of polycrystalline films is of the order of one or two unit cells only, the diffraction pattern is very diffuse and the crystal type cannot be readily identified by examination of the diffraction peak sequence. A number of authors have calculated the shape of the interference function si(s) for small crystallites. The procedure is simply to count the number of bond lengths of different sizes within a crystallite of given size and to calculate i(s) from the Debye equation. An implicit assumption is made that the microcrystallites are randomly oriented and intercrystallite interferences are neglected. Figure 2 shows two typical calculated curves for fcc crystallites with, for comparison, an experimental

curve for a deposit of Ni of approximately 10 Å mean thickness (20). Calculations for fcc crystallites have been made by Germer and White (21) and Grigson and Barton (22), for bcc crystallites by Morozumi and Ritter (23), and for diamond crystallites by Tsiensuu et al. (24). Such curves illustrate very well the diffuseness of the diffraction pattern resulting from small particle size. It should be noted that particle size estimation from line broadening formulae become unreliable in this extremely small size range. Attempts to fit experimental curves are usually rendered difficult by the need to take into account a range in microcrystallite size, and by the neglect of interference effects across boundaries between crystallites in the small crystallite calculations.

The rdf technique is of considerable value in examining such films. Figure 3 shows the rdfs obtained from the curves of Fig. 2. The remarkable number of sharp peaks can be noted and comparison may be made between the rdf in 3a of one of the theoretical intensity curves and the rdf of the experimental curve, 3b. There is little doubt in this case that the very thin deposit consisted largely of fcc microcrystallites.

The case of randomly oriented isolated, i.e., noncontiguous, particles is of special interest since many atoms are now located at the surface rather than in the interior of a particle. Atoms at the surface have a smaller number of neighbors than when located within the bulk of the material, and hence the coordination numbers indicated by the rdf may be much decreased, since they are averaged over all atoms. A decrease in coordination

number is also to be expected if a material contains a great many voids. Figure 4 shows a plot of calculated mean number of nearest neighbors about any atom for isolated, near cubic, fcc crystallites of varying size. It may be shown that the mean coordination numbers for fcc crystallites of rectangular block shape having sides of length ℓ_1, ℓ_2, ℓ_3 is given by

$$C_{123} = \frac{1}{3}\left[(C_1C_2)^{1/2} + (C_2C_3)^{1/2} + (C_3C_1)^{1/2}\right]$$

where C_1, C_2, C_3 are the mean coordination numbers for cubes of edge dimensions ℓ_1, ℓ_2, ℓ_3.

A particularly interesting examination of very thin deposits of lead films has been given by Heritage and Tillett (25), in which it was found that films of 8.5 Å mean thickness showed good correspondence with curves calculated for fcc crystallites, while thinner films, of 2 Å mean thickness, did not. Instead, the rdf was found to agree very well with curves calculated for close-packed icosahedral clusters. Such clusters require some few percent bond length distortion but provide a very close-packed, but "non-crystalline," arrangement that may be stable for small clusters (26). This is an important result that shows the great potentiality of the rdf technique for the investigation of atomic configurations in small nuclei formed during the initial stages of film deposition.

3. Experimental Requirements

An important parameter required for the calculation of the rdf is the density ρ_o (average number of atoms/A^3). Very typically, measurements indicate a value of ρ_o some 5 or 10% smaller

than the value for crystalline material of the same composition. Moss and Graczyk (27) have noted that the decrease in density of amorphous Si films was associated with internal voids as evidenced by appreciable electron small angle scattering. As the films were annealed the small angle scattering decreased, indicating an increase in density for the films. It seems probable that density values that are unusually low may be due to the presence of microscopic cracks or voids. This raises the question as to the correct value of ρ_o to be used in the calculation of the rdf. It may be shown that very approximately the change ΔC in nearest neighbor coordination number due to a change $\Delta\rho_o$ in density arising from the presence of internal voids of linear dimension ℓ is given by $\Delta C/C = (\Delta\rho_o/\rho_o)d/\ell$, where $d \simeq \rho_o^{-1/3}$, i.e., an interatomic distance. C and ρ_o are values of coordination number and density in the absence of voids. For a film to show appreciable small angle scattering, void size must be considerably larger than d and hence the actual mean coordination number in the material is little affected by the presence of the voids. If the voids shrink to atomic vacancy size, then $\Delta C/C$ is of order $\Delta\rho_o/\rho_o$; in itself not a large change, bearing in mind the experimental uncertainty in ρ_o and in the transformed curves. The value of ρ_o to be employed should therefore be that intrinsic to the amorphous material with exclusion of effects due to macroscopic voids.

Inclusion of significant small angle scattering intensity in the diffraction data has the effect of adding a density contribution to G(r), i.e., the slope of the G(r) curve at small r is

found to be $-4\pi r\mu\rho_o$ instead of $-4\pi r\rho_o$, where μ is somewhat less than unity. This effect has been noted by Moss and Graczyk (27) and by Denbigh and the present author (28). A more complete discussion of the influence of neglected small angle scattering in rdf analysis has been given by Cargill (29).

A possible check on the value of density may be obtained in the case of Si and Ge by comparing the small shift in the electron energy plasma loss peak due to the excitation of long range density fluctuations in the outer shell electron population. In the simplest theory the loss peak occurs at an energy proportional to the square root of the valence electron density. If it is assumed the difference in peak position between crystalline and amorphous films is due entirely to a bulk density change, then the density deduced for the amorphous Si or Ge films is only 3 to 5% less than the crystalline value, as noted by Richter and collaborators (30). Unfortunately, this technique is not of general applicability since plasma loss peaks are rather broad in many materials.

It should be noted that the successful application of the Fourier transform technique requires intensity data of reasonable accuracy from small to large scattering angles. The theory assumes that there is no preferred orientation of scattering units, that multiple scattering (31) and inelastic scattering contributions are negligible, and that small angle scattering effects are properly treated.

The question arises, what value of maximum scattering angle gives an acceptable resolution of the peaks in the rdf? It may

be said briefly that the ripples of the si(s) function should have become largely attenuated at the end of the angular range. Whether this is achievable in practice depends on the sharpness of the first peak in the rdf and on the limitations of available equipment. The shape of the peaks in the rdf, as mentioned previously, are determined by a convolution product, and the validity of peak shape should be established by deconvolution of the curve.

For observation with an electron beam of energy 50 kev, films should be thin, of order 100 Å or less, and an electron energy filter should be used to reject inelastically scattered electrons. This requirement has been met only in very few cases; more usually, numerical corrections are made to the data. The data are divided by $F^2(s)$ and are normalized by noting that $I(s)/F^2(s)$ tends to a constant value $N\Sigma x_i f_i^2(s)/F^2(s)$ at large s; hence a value for N may be obtained that also takes into account instrumental gain factors (32).

The electron scattering factors are available in tabulated form and are considered to be reliable for large values of s, but the behavior at small s is less well established. An extensive discussion of scattering factors in electron diffraction may be found in the article by Seip (33).

Finally, si(s) is calculated from

$$si(s) = s[I(s) - N\Sigma x_i f_i^2(s)]/NF^2(s).$$

The transform of g(s)si(s) is then carried out where g(s) is a slowly varying function over $o < s < s_{max}$, is zero for $s > s_{max}$,

and is equal to unity at s = 0.

The result is a sum of convolution products involving distribution functions $\rho_{ij}(r)$, where $\rho_{ij}(r)$ gives the number of atoms of type j per unit volume at distance r from an atom of type i. In general, the diffraction experiment does not provide sufficient data to determine the individual ρ_{ij} distributions. This serious difficulty does not arise in the case of elements and the transform gives then a convolution product involving a single distribution function $4\pi r[\rho(r)-\rho_o]$ and the transform of g(s). Thus, even in the case of elemental amorphous films the transform procedure does not immediately give $4\pi r[\rho(r)-\rho_o]$ and hence permit the calculation of the rdf $4\pi r^2\rho(r)$. Although this point is well recognized, it is not made clear in the literature where almost invariably no distinction is drawn between the convoluted radial distribution function and the true rdf.

A very useful technique for obtaining a deconvoluted rdf has been employed by Mozzi and Warren (34) in an (x-ray) re-evaluation of the structure of vitreous silica. In this method pair functions are obtained by calculating the transform of a theoretical si(s) arising from the interference between atoms of given type and constant interatomic spacing. The calculation is repeated with various degrees of thermal broadening and the transform is carried out over the same range as that employed in treating the experimental data. Thus the area and shape of a peak due to interference contributions between atoms of several types can be compared and employed to analyze the rdf. Full details are to be found in the book by Warren (11). The importance of due attention

to the analysis of the data using deconvolution techniques cannot be overemphasized when detailed information is to be extracted from the rdf. This procedure combined with instrumentation in which intensities are recorded electrically, and incoherent or inelastic contributions are rejected experimentally, represents a major improvement in rdf analysis.

III. EXPERIMENTAL TECHNIQUES

1. Photographic Recording of Intensity

The conventional technique of recording electron diffraction patterns by exposing photographic plates to the scattered electron beam suffers from several major disadvantages when applied to the measurement of diffuse patterns:

i) The plate records inelastic as well as elastically scattered electrons, making necessary corrections for inelastic background.

ii) Intensity varies across the pattern by several orders of magnitude.

iii) It is necessary to calibrate the photographic plates so that the relation between optical density and exposure to electron beam is reliably known (35,36).

Many materials have been examined, however, by photographic recording techniques and much valuable information has been obtained. In some cases, however, the experimental rdfs have been analyzed into a series of overlapping sharper peaks in order to improve on the obtained experimental resolution. It must be

cautioned that this procedure requires high fidelity of peak shape, and hence slowly varying systematic errors in the intensity data must not be permitted.

2. Electronic Recording Technique

An advance in the precision of intensity measurement was brought about by the development of the scanning or direct recording technique. In one type of instrument developed by Grigson and coworkers at the University of Cambridge (37), and by Grigson and the present author at the Bell Telephone Laboratories (38,39), the scattered electron beams are deflected to and fro across a very small aperture by a pair of magnetic coils situated beneath the specimen. Electrons entering the aperture pass through an electrostatic filter, which rejects electrons that have lost more than a few volts in energy. The transmitted electrons are collected by a Faraday cage or other type of detector. This is shown schematically in Fig. 5. A comprehensive review of the electronic recording technique and its application to thin film studies has been given by Grigson (40).

Direct recording techniques and filters for electron energy analysis have been pioneered by Molensteht (41), Boersch (42), Simpson and Marton (43), Burggraf and Goldsztaub (44), and Raether and coworkers (45), but in these cases attention has been directed primarily to the study of scattering mechanisms rather than to the analysis of film structure. An energy filtered direct recording arrangement incorporated into an electron microscope has been

described by Moss and Graczyk (46). This is a very powerful technique combining both electron microscopy and direct recording electron diffraction. A commercial direct recording high vacuum energy filtered diffraction unit is now available (47) and an electron microscope direct recording energy filter accessory is available from AEI (48).

The direct measurement of an intensity profile of elastically scattered electrons makes this type of instrument an almost ideal tool for the investigation of diffusely scattering materials. The advantages to be gained from such an instrument are

i) experimental elimination of incoherent, i.e., inelastic scattering,

ii) very good comparative measurement as some parameter, e.g., time, temperature, is varied, and

iii) extension of measurements to a greater angular range.

It is to be noted that the major improvement to be expected in the rdf lies in the more reliable peak shapes and in better peak resolution rather than in any radical change in major features such as nearest neighbor distance.

IV. REVIEW OF RDF MEASUREMENTS

In this section rdf work on thin films is reviewed. Attention has been given to the electron diffraction studies of films of a few hundred Å or less prepared by vapor deposition techniques. Work on much thicker films, e.g., many microns in thickness,

utilizing x-ray diffraction has been included in some cases for comparison with the electron diffraction results. It is hoped that this compilation will convey a useful impression of the work carried out on the structure of amorphous films, although the major part of this work has been carried out using photographic techniques, and only in recent years has the energy filtered electron diffractometer become available. Generally speaking, little attention has been given to termination broadening of rdf curves and deconvolution has been seldom attempted. Where appropriate, similar materials are grouped together under a common heading to avoid repetition.

1. Elements

a. Amorphous Metals - Fe, Cr, Ti, Mn, Co, Ni, Pd, Y

While early work on the deposition of metals onto very low temperature substrates had indicated that the resulting films were polycrystalline (49,50), a number of papers have indicated that a diffusely diffracting film may be obtained, at least during the initial stages of deposition; the film subsequently crystallizes as the temperature is allowed to rise or upon other treatment (52,53). Fujime (54,55) reported obtaining amorphous films of Fe, Cr, Ti, Mn, Co, Ni, Pd and Y by low temperature vapor deposition, and concluded from photographic electron diffraction observations that the local order is essentially liquid-like. The diffuse scattering from very thin films may be due to either fine grain size or to atomic disorder. A particularly interesting observation has been reported by Heritage and Tillett (25) in which thin films of Pb were grown on carbon films inside

a direct recording energy filtered system, and rdfs were obtained at various stages of film growth as shown in Fig. 6. While films of mean thickness greater than 8 Å appeared to consist of very small crystallites, the rdfs from thinner films could not be so directly interpreted. Intensity profiles were recorded continuously as thickness was increased, and in this way a comparison between rdfs could be made from data obtained and treated in a similar manner, lending considerable credence to the changes observed. However, it was found that an excellent fit to the rdfs could be obtained by assuming that the atoms formed close packed polyhedral clusters. Such clusters are more densely packed than the fcc structure but involve bulk strains that make the formation of large clusters of this type energetically unfavorable (26). Grigson, Dove and Stilwell found that thin films of Fe grown inside a direct recording energy filtered electron diffraction system (56) consistently gave diffuse diffraction patterns; crystallization occurred at a critical thickness, but the effects of impurities or temperature were not investigated. Later rdfs of these films shown in Fig. 7 were in approximate agreement with those of Fujime, however, the sequence of peaks was interpreted as platelets of close packed planes, e.g., fcc {111} planes randomly stacked. It is of interest to note that Fe possesses a high temperature fcc phase and high pressure hexagonal phase, and that epitaxial fcc films have been obtained under certain conditions (57). Since the amorphous films were found to be ferromagnetic with magnetization considerably less than that of crystalline iron, consideration of the properties of the several

phases of iron (58) suggests that a model for the local order based on a highly faulted fcc structure would be most probable. The rdfs show a close resemblance to that reported by Wagner (60) for splat cooled Fe with some 20% carbon and phosphorus additions, shown in Fig. 8. On crystallizing the films, only α-Fe was found with no sign of carbides or other compounds, differing in this respect from the splat cooled materials.

Antimony and Arsenic

Geiling and Richter (61) prepared thin films of arsenic by sublimation and chemical deposition of very fine particles. Electron and x-ray diffraction patterns showed only diffuse haloes although crystallization could be brought about by heating to 285°C. The nearest neighbor distance was found to be 2.40 Å instead of the crystalline value 2.51 Å, with a coordination of 3.2 in good agreement with the crystalline value 3.0. Other distances were in approximate consistency with interatomic distances in crystalline arsenic, except that the second nearest distance of 3.15 Å appeared to be absent from the rdf. The third neighbor distance had a coordination of 9 instead of the crystalline value 6. In later work Richter and Gommel (62) obtained agreement with the crystalline nearest neighbor distance, but the second neighbor distance occurring in crystalline material was absent or much reduced in the rdf. The authors suggested that the amorphous films consist of regions of ordered layers similar to the layers occurring in the crystalline form. This work was further reviewed by Breitling (63). The structure of crystalline arsenic is a layer structure consisting of three

coordinated arsenic atoms. X-ray studies on arsenic films have been reported by Richter and Breitling (64) and more recently by Krebs and Steffen (65). The latter authors report a nearest neighbor distance of 2.49 Å and coordination 3.0. This paper also contains a discussion of local order in "explosive" antimony. The effect of impurities of various types in stabilizing or devitrifying amorphous antimony films is reported in several papers by Palatnik and Kosevich (66).

Bismuth and Gallium

In a remarkable series of experiments by Buckel and Hilsch (49), Bulow (50) and Bulow and Buckel (51), films of Bi and Ga deposited onto very low temperature substrates were found to be superconducting with transition temperatures of 6° and 8.4°K. The electron diffraction patterns taken at cryogenic temperatures were extremely diffuse until film temperature was allowed to rise to about 15°K whereupon crystallization occurred. The bismuth films were then no longer superconducting and the gallium films had a new transition temperature of 6°K. Further heat treatment lowered Tc to 1.07°K.

The diffuse diffraction patterns of the vapor quenched films were analyzed by Leonhardt et al. (67) and later by Richter (68) and Richter and Breitling (69). The amorphous films were found to have a close packed structure very similar to that of liquid bismuth. Work by Fujime (70) is consistent with this result; peaks in the rdf were located at 3.28, 4.5 and 6.5 Å with nearest neighbor coordination of 5.6. This is somewhat smaller than the value 6.7 found by Richter and collaborators, but both values are

comparable with results obtained by Takagi (71) on supercooled liquid bismuth films where the nearest neighbor coordination varied from 8.0 at 400°C to 6.0 for supercooled films at 110°C. This work was carried out using 50 kv electrons in reflection and is possibly unique in that rdfs were calculated from reflection diffraction curves. Numerical corrections applied to the data are considerable, due to the large background of inelastic secondary electrons.

Gallium appears to behave very similarly and is discussed along with bismuth in many of the above papers. Presumably the occurrence of superconductivity at elevated transition temperatures is connected with an increase in density compared with the normal structures. Bismuth contracts on melting and also contracts under high pressure to form superconducting phases. Richter and Breitling in later papers proposed that the amorphous phase is stabilized by the simultaneous occurrence of both close packed and layer-like regions in the films.

Beryllium

As in the case of bismuth, thin films of beryllium prepared by deposition onto substrates at cryogenic temperatures become superconducting with Tc ~8°K or 6°K depending on preparation conditions. Fujime (72) deposited beryllium films over 500 Å in thickness onto collodion and carbon film substrates held at 4.2°K. The vacuum level at the specimen was reported to be approximately $2 \cdot 10^{-7}$ torr. Very diffuse diffraction patterns were obtained photographically with the specimen at cryogenic temperature. The onset of crystallization was noted when the temperature was

allowed to rise to about 130°K. Corrections to data were applied for substrate scattering and incoherent background, and the rdf was calculated using a gaussian termination function. Peaks in the rdf were found at 2.25, 3.7 and 5.8 Å, with a nearest neighbor coordination of 11, this being consistent with a local order similar to that in the cph crystalline structure of beryllium. The author concluded that the films were not microcrystalline largely on the basis of the scarcity of peaks in the rdf and their broadness. This is not a very sure criterion, however, in view of the uncertainties surrounding the data and the use of a termination factor.

Boron

Katada has examined films of boron, a few hundred Å in thickness, using electron diffraction (73). The films were deposited onto rocksalt in a vacuum of approximately 10^{-5} torr. The photographic plates showed diffuse rings only with eleven haloes out to $4\pi\sin\theta/\lambda \approx 23\ A^{-1}$. A correction factor was applied to obtain the intensity of elastically scattered electrons. Several techniques were employed to compare the first peak of the rdf with that which would be expected for nearest neighbor distances and coordination corresponding to the icosahedral structure in the crystalline forms of boron. It was concluded that a local atomic order corresponding to that in the crystalline phase would be quite consistent with the rdf. It was necessary, however, to fit the first peak to five subsidiary peaks and, in addition, some indications that multiple scattering may have influenced the data were reported. A bond length of 1.47 Å arising as part of the

analysis of the first rdf peak was considered as possibly due to boron-oxygen bonds in the films.

Carbon

Carbon films, typically prepared by subliming from high purity rods in a vacuum, have been much used for specimen supports in electron microscopy. It has long been known that such films show a graininess when observed at the highest attainable magnification. This graininess has been variously ascribed to a phase contrast mechanism, and to microcrystalline contrast. The diffraction pattern from carbon films is very diffuse and has been the subject of study by Kakinoki et al.(74), Boiko et al.(75,76), and the present author and collaborators (77).

Kakinoki et al. examined films of 100 Å thickness using photographic techniques and a data range out to $4\pi\sin\theta/\lambda = 27$ A^{-1}. Background corrections to data were applied that were particularly important at low angles. The authors are careful to distinguish between the rdf obtained by transforming data over a finite range and the actual rdf for the material. The first peak in the rdf indicated an interatomic distance of 1.50 Å lying between the values 1.42 and 1.54 Å for carbon-carbon distances in graphite and diamond, respectively. The first and second peaks were therefore decomposed into overlapping subpeaks and the author concluded that the films actually contained regions of both graphitic and diamond ordering. This aspect was discussed further by Kakinoki in a later paper. More recent work by Boiko et al. (75,76) using energy filtered electron diffraction with electronic recording failed to find any diamond type of ordering and found a graphitic

local ordering. This result was also obtained by the present author as shown in Fig. 9. More recent observations on heat treated films by Heritage et al. (78) confirm this and show a gradual sharpening of peaks in both the intensity and rdf curves, indicating increasing graphitic ordering. Work on bulk glassy carbons formed by pyrolysis of polymeric material may well show the presence of other types of carbon bonds (14,79,80).

Hexagonal cells have been resolved in extremely thin films by Heidenreich using extremely high resolution microscopy (81) indicative of a graphitic microstructure, although it is to be noted that a further hexagonal structure of carbon has been reported (82). Rudee has also reported on a microcrystalline structure in carbon films using high resolution dark field electron microscopy, a difficult but extremely promising technique for structural observations on amorphous films (83). A similar observation has also been made by Tanaka (84).

Gallium (see Bismuth and Gallium)

Germanium and Silicon

Amorphous films of germanium (63,67,84-97) and silicon (27, 92) have been the subject of many investigations leading to a variety of conjectures concerning the details of local atomic configurations. Richter and collaborators (67) examined films under different conditions using electrons and x-rays and noted that the tetrahedral coordination between atoms characteristic of crystalline Ge and Si was preserved in the films, as evidenced by the first and second peaks in the rdf. Higher order peaks did not fit a microcrystalline model and the authors proposed in

several papers models based on atomic layers, chains of rotated tetrahedra and regions of relative order separated by disordered material. In much later work the authors have elaborated upon these models, choosing to distinguish between structures on the basis of fine differences between rdfs which are not in themselves entirely free from defects (63).

Coleman and Thomas (92) report on silicon films examined by electronically recorded electron diffraction, without energy filtering. The authors also noted that the peaks in the rdf may be fitted to microcrystalline models, except that the third peak (very strong in the crystalline case), is considerably attenuated. The authors proposed a structural model, referred to as the "amorphon," in which atoms join in five-sided rings to form a follow spherical cavity with bonds extending outwards from the cavity. A rough fit to the rdf was obtained by averaging over local microcrystalline and amorphon configurations. This geometrical curiousity, however, offers little advantage over the twisted chain of tetrahedra model.

In more recent work Grigorovici and collaborators (88) have given an extensive discussion of the problem of building a glassy network using the tetrahedron as a unit and introduced the concept of packing together Voronoi polyhedra to generate a three-dimensional structure. The major feature of this work is the mixing of staggered and eclipsed configurations in which adjoining tetrahedra are rotated 0 or 180° relative to their crystalline arrangement.

Work by Moss and Graczyk (27) on Si films using energy filtered electron diffraction, and by Chang and the present author

(93) on Ge films, has given very similar rdfs for the two materials as shown in Figs. 10 and 11. Figure 11a shows the rdf obtained by carrying out the transform with no termination function; termination ripples are prominent. Figure 11b shows the final rdf obtained by numerical deconvolution of 11a. In both cases the first peak of the rdf is found to be very sharp. The spread in the nearest neighbor interatomic distance is largely due to atomic vibrations and static bond distortions appear to be quite small, when allowance is made for termination effects. The nearest neighbor distance is not significantly different to that in the crystalline material. The second peak in the rdf is broader than the first; this distance involves the tetrahedral bond angle and it was estimated that a distortion of bond angle by about 15 or 20° would account for the spread in interatomic distance. The second peak also has a coordination very close to the crystalline value 12. The next peak in the rdf depends on the relative fitting together of adjoining tetrahedra. In the crystalline case this is a strong, coordination 12, well-defined peak, but in the films this is considerably spread out and is scarcely apparent as a peak in the rdf, although a small peak is to be seen at a somewhat greater distance. This peak could arise from a relative rotation of 30° of the tetrahedra with respect to each other, and possibly in other ways as well. Attempts to fit the rdfs with microcrystalline models including other structures such as wurtzite and the Ge high pressure phases have not been successful (94).

It is of interest to note that Polk (95) has constructed a

mechanical model in which a three-dimensional network is built up using tetrahedral coordination with appropriate angular distortions of the linkages. The calculated rdf for this structure is in the form of a histogram, but is consistent with the experimental rdf. Henderson and Herman (96) have generated models by computer with similar results. An rdf of Ge with high peak resolution obtained by x-ray techniques has been reported recently by Shevchik (96). In all of this work a picture emerges in which the tetrahedral bonding is preserved with little distortion of the strong nearest neighbor bonds but in which some bond angle distortions occur. Little definitive can be said about more long-range structural details, although work by Brodsky and Title (98) using esr techniques suggests that rather few dangling bonds are present and that esr signals are due to internal voids. While models based entirely on microcrystalline regions do not appear to fit the rdfs, the presence of a substantial proportion of microcrystalline regions cannot be entirely discounted.

Rudee, using high resolution dark field electron microscopy (99) in fact reports on the observation of small crystalline regions in amorphous Ge and Si films and suggests that most of the material is contained within the ordered regions. It is of interest that even in these (structurally) relatively simple materials, which have been examined by many investigators, uncertainty still exists on the basic character of the amorphous structure. It is a possibility that variations all the way from a completely three-dimensional glassy network structure to one containing a high proportion of ordered regions may exist depending on

preparative conditions and thermal history. The best presently available rdf data do not rule out the possibility of crystalline regions existing in the films but do indicate that the proportion of diamond crystalline regions in those films examined cannot have been very large.

An important structural technique utilizing x-ray absorption edge fine structure has recently been applied to a comparison of amorphous and crystalline Ge by Sayers, Stern and Lytle (100). An atomic distribution function is obtained directly from the data, the results being in reasonable agreement with those of the rdf investigations. This technique is likely to be of special importance for the examination of compounds since the environment of each type of atom may be probed separately.

Selenium

Crystalline Se exists in several modifications, the α-monoclinic structure consisting of Se_8 ring molecules and a trigonal structure in which the Se atoms link to form helical chains. In both cases the selenium atoms form strong bonds with two neighbors, but the rings or chains are only weakly bound together by long-range forces. Rdf curves of vitreous selenium have been reported by a number of workers using both x-ray and electron diffraction techniques (101-113). There is little question that the nearest neighbor covalent bonding with two-fold coordination is preserved in the glassy stage; most of the interpretations of the rdfs have hinged on deducing the presence of rings or chains, singly or together. Hendus (103) compared his results with the structure of crystalline α-Se. Richter and collaborators (104-107)

over a number of years proposed a model based on a structure composed of layers of selenium chains. In other work with Grimminger and Greninger (108), a chain structure is favored at room temperature and six-membered rings at -180°C. Neutron diffraction by Henninger et al. indicated a mixture of chains (109). Kaplow et al. (110), using careful x-ray techniques, compared vitreous and polycrystalline hexagonal selenium prepared by both casting and vapor deposition techniques. Rdf curves for the monoclinic α and β forms were calculated from the crystal structures, including allowance for atomic thermal motion. The authors concluded that a combination of microcrystalline structures would not reproduce the rdf exactly, and carried out an interesting computer exercise to disorder the known crystal structures to try to improve the fit with the rdf. Examination of the computer generated atomic positions revealed that the best fit was obtained with slightly distorted ring structures with some small proportion of chains. This is in agreement with infrared work by Lucovsky (111,112) in which a strong correlation was found between amorphous Se and the Se_8 ring structure crystalline form. It may be noted that Andrievskii et al. (113), using photographic electron diffraction, obtained rdfs at various temperatures around room temperature and above. They conclude that Se_8 rings exist at 20°C, short chains at 70°C and a mixture at intermediate temperatures. This is a very interesting result that remains to be verified with other techniques.

2. Compounds

a. Metals

Vapor deposition of certain metallic alloys onto cooled substrates has been found to produce films that give an extremely diffuse diffraction pattern. Details of this work have been discussed by Mader and collaborators (114) and may be compared with the extensive results obtained by forcibly splat cooling bulk alloys onto cooled substrates reported by Duwez and coworkers (115).

Ag-Cu

Ag and Cu were deposited simultaneously onto a substrate at 77°K and the films were examined by electron diffraction. From rdf analysis of the intensity curve, Fujime (116) concluded that the film was in an "amorphous state" but models for the local atomic configurations were not discussed. A detailed x-ray analysis of 1μ thick films of vapor quenched Ag-Cu alloys by Wagner et al. (117), however, led to the conclusion that their films consisted of fcc microcrystallites with particle size of order 15 Å.

Ag-Ge

Films of thickness from 1 to 3μ were prepared by coevaporation of Ag and Ge into substrates at liquid nitrogen temperature. Light and Wagner (118) investigated films of several compositions and found that they consisted of Ag solid solution and Ge. The Ag phase was thought to be polycrystalline with particle size of order 15 Å. Line broadening calculations were consistent with this result.

Au-Co

Fujime (119), using photographic electron diffraction, reports on the rdf of a vapor quenched Au-Co film. The fairly broad first peak in the rdf was thought to be due to overlapping Au-Au, Co-Co and Au-Co distances. Other peaks in the rdf were greatly attenuated indicating little order in the film. The area of the nearest neighbor peaks was found to be 5.5 in considerable variance with the figure of 12 or slightly less that might be expected for a close packed structure.

Cr-Ni

The structure of nickel-chromium alloy films has been examined by Bicknell (120) using electron microscopy and electron diffraction. The films were prepared by flash evaporation onto room temperature substrates in a vacuum of 10^{-4} torr. The compositions were similar to those used in alloy film resistors. It was found that the rdfs could be analyzed in terms of an assembly of fcc or bcc crystallites or a mixture of both. As chromium content was increased, the deposited film became less evidently crystalline and crystal growth during annealing decreased. Growth of fcc crystallites occurred at 300 to 400°C, while at 600°C Cr_2O_3 formed. Evidence for Cr-O bonds was not found in the rdfs, taken prior to heat treatment.

BiPb

Bismuth-lead films containing 12% Bi were vapor quenched onto substrates at 4.2°K inside an electron diffraction camera. Fujime (72) found that the films gave a very diffuse pattern and were stable up to 8.9°K, when transformation to an fcc structure

occurred. Peaks in the rdf are reported at 3.25, 5.2 and 7.8 Å with a nearest neighbor coordination number of 8.5. The local order is not commented upon but the results of Sharrah and Smith (121) on liquid lead at 550°C using neutron diffraction are noted for comparison. In this case the nearest neighbor distance was 3.40 Å with a coordination of 9.5.

FeNi

Fujime (54) examined films of Fe-50% Ni deposited onto substrates held at a low temperature. Rdfs were obtained by photographic electron diffraction and peaks at 2.64, 4.4, 6.6 and 8.7 Å were noted. The first coordination number was found to have a value 8, and the structure was thought to be "liquid-like" but this was not elaborated upon.

b. Semiconductors

As_2S_3

As_2S_3 films were evaporated onto cold rock salt substrates and were examined by photographic electron diffraction techniques. The rdf reported by Tatarinova (91) shows a split first peak and negative overshoot. The author concludes that the short range order in the films is similar to that in the crystalline structure (122) where the nearest neighbor coordination numbers are 3 and 2.

As_2Se_3 and As_2Te_3

Andrievskii et al. (123) have prepared films of As_2Se_3 and As_2Te_3 of thickness from 500 to 1,200 Å by evaporation in vacuum onto cellulose nitrate support films. The support films were dissolved in acetone and the remaining films were examined by

photographic electron diffraction. The films were then given mild heat treatments. Nearest neighbor coordination numbers were found to vary with temperature between the values 4 and 7, and nearest neighbor separation was close to that obtained from the sum of the covalent radii. Considerable negative overshoot is evident in some of the rdfs, however, which is not surprising in view of the great thickness of the films, and detailed interpretation of the results should be carried out with caution.

GaAs

GaAs films were prepared by vapor deposition onto room temperature plastic substrate films at room temperature and were examined by Tatarinova using photographic electron diffraction (91). The rdf curves showed maxima at 2.53 and 4.25 Å with coordinations of approximately 4 and 10, respectively. It was concluded that the tetrahedral atomic configuration characteristic of the crystalline form is retained in the films.

GaSb

Mikolaichuk and Dutchak (124) deposited GaSb films to a thickness of 300-700 Å onto room temperature cellulose nitrate substrates in a vacuum of 10^{-5} torr. The substrates were then dissolved and electron diffraction patterns were recorded photographically. Amorphous films were obtained regardless of evaporation rate. It was concluded that the local order was tetrahedral as in crystalline GaSb with nearest neighbor distance approximately as in the crystalline phase. Heat treatment up to 90°C had little effect on the films.

GaSe

Amorphous films of GaSe have been examined by Tatarinova (125) using photographic electron diffraction. The films were reported to be very stable. The rdf showed maxima at 2.40 and 3.75 Å which may be compared with the interatomic distances 2.33, 2.48, 3.75 and 3.84 Å in the crystalline form. Coordination numbers of 6 and 12 are reported for the first two peaks; however, the rdf shows negative overshoot and values for coordination numbers are not likely to be reliable in such a case.

Ga_2Se_3 and Ga_2Te_3

Thin films of Ga_2Se_3 and Ga_2Te_3 were prepared by Andrievskii et al. (126) by evaporation onto nitro-cellulose support films which were then removed by dissolution. Photographic electron diffraction was employed to obtain rdfs. The structure of the films was found not to depend on rate of evaporation or thickness, but did change upon heat treatment. The nearest neighbor interatomic distance was found to be 2.25 Å, rather less than the shortest Ga-Se interatomic distance 2.34 Å in the crystalline form. The nearest neighbor distance and coordination was found to decrease with heat treatment to 200°C, but at higher temperatures new peaks occurred. Heat treatment of Ga_2Te_3 films increased the degree of order and the films had a local order comparable with crystalline Ga_2Te_3 after heat treatment at 50°C.

Ge_xSe_{1-x}

Films of Ge_xSe_{1-x} have been examined by Fawcett et al. (127) and by the present author and collaborators (128), both groups using electron diffraction with energy filtering and

electronic recording. A typical intensity curve is shown in Fig. 12. The rdf curves are consistent with a random network in which the Ge and Se atoms exhibit four- and two-fold coordination with interatomic separation approximately equal to the sum of the covalent radii, which in this case predicts bond lengths of 2.44, 2.39 and 2.34 Å for Ge-Ge, Ge-Se and Se-Se neighbors. The first peak in the rdf does not allow a determination of the relative number of the different types of bonds and it is therefore very difficult to decide whether bonds between unlike neighbors are favored. A $GeSe_2$ glass in the ordered case would be a structural analogue of vitreous silica. Interestingly, the structure of crystalline $GeSe_2$ is reported to be a distorted CdI_2 layer structure (129) in which each layer consists of Ge atoms surrounded by 6 Se atoms while each Se has 3 Ge neighbors, resulting in a nearest neighbor coordination of 4 within the layers. GeSe, the other crystalline compound occurring in the equilibrium phase diagram (130), has a distorted cubic structure with several nearest neighbor bond lengths. Mikolaichuk and Kogut (131), however, using photographic electron diffraction, obtained rdfs of amorphous films of GeSe that had a first peak at 2.60 Å and a nearest neighbor coordination of approximately 6. These authors concluded that the local order was the same as in crystalline GeSe.

In a detailed study of $GeSe_{0.7}$ and $GeSe_{1.5}$ films and their response to minor heat treatment, Molnar (132) has found very pronounced changes in the intensity profiles and in the rdfs, indicating an increase in nearest neighbor coordination and the occurrence of bonds at about 2.9 Å in addition to the major bond

length of 2.4 Å. The intensity changes in the case of GeSe are shown in Fig. 13 and the resulting rdfs are shown in Fig. 14. These changes were interpreted in terms of the nucleation of the crystalline phases, and were strongly influenced by the use of copper mesh support.

Lytle and collaborators (133) have obtained atomic distribution curves for Se and Ge atoms about a Ge as center and also about an Se atom as center, using x-ray absorption edge data. The curves shows the Se atoms lying at two nearest neighbor distances as shown in Fig. 15. This technique, particularly when combined with rdf data, promises to be of extreme importance for the analysis of multicomponent materials.

Ge_xTe_{1-x}

The electronic and other properties of films of Ge_xTe_{1-x} and related more complicated compounds have been the subject of extensive investigations in recent years. In tellurium-rich compositions, bulk glasses may be obtained while amorphous films may be prepared at almost all compositions depending on substrate temperature. X-ray work by Bienenstock and collaborators (134, 135) has shown that structural models in which Ge and Te possess four-fold and two-fold coordinations and in which the effective atomic radii are close to the covalent radii, are consistent with the rdf curves. Intensity and rdf curves are shown in Figs. 16 and 17. A similar result for Te-rich compositions was obtained by Luo and Duwez (136). This result was also found to hold for films very close to the 50 at.% composition, i.e., GeTe, and it was concluded by Bienenstock and collaborators that a local order

characteristic of crystalline GeTe was not present in the films. The structure of GeTe is distorted cubic (138), becoming cubic at high temperatures with an expanded nearest neighbor distance of 3.00 Å and a coordination of 6.0, which may be compared with the result for films of 2.70 Å and coordination of order 3. Dove et al. (137) examined very thin sputtered films of GeTe using energy filtered electronically recorded electron diffraction and also found a nearest neighbor configuration different from that of crystalline GeTe. In this case, a nearest neighbor distance of 2.65 Å and coordination of order 4 was found and a tetrahedral atomic configuration was suggested. In later work a smaller value of coordination was obtained although the actual value appears to be quite sensitive to electron beam exposure or thermal treatment of the films (139). Mikolaichuk and Kogut (131), on the other hand, examined amorphous films of GeTe (and GeSe) using photographic electron diffraction, and obtained a nearest neighbor coordination of order 6. It was concluded that the local order was therefore similar to that in crystalline GeTe, although the mean nearest neighbor separation was found to be 2.75 Å.

Interest in the chalcogenide glasses stems from their potential application in electronic switching and other devices and in their use as infrared transparent optical materials (140). Adler et al. (141) have carried out NMR measurements on $GeTe_4$ bulk glasses and have discussed the degree of ionicity of the primarily covalent bonds in the material. Betts et al. (142) have reported x-ray absorption edge and photoemission studies and conclude that the bonding in these alloys is primarily covalent.

Crystallized samples and crystalline GeTe, GeSe and GeS showed edge shifts different from those obtained from the glasses. Rustum Roy and collaborators have reported on the important phenomenon of phase separation (143) in these materials. Phase separation in films has not been clearly established, however.

InAs

Films of InAs, prepared by deposition onto rock salt, have been examined by Tatarinova (144), using photographically recorded electron diffraction patterns. The radial distribution curves show peaks at 2.5 and 3.8 Å with a nearest neighbor coordination of order 4. This does not agree completely with the tetrahedral configuration in crystalline InAs where the distance between unlike atoms is 2.61 Å.

InSe

Films deposited onto room temperature rock salt substrates were considered by Tatarinova and Kazmazovskaya (145) to be microcrystalline although detailed calculations were not presented. The first peak in the rdf curve was interpreted as consisting of two overlapping peaks centered on 2.60 and 3.15 Å; this may be compared with the 2.50 and 3.16 Å distances occurring in the crystalline form (146).

In_2Se_3 and In_2Te_3

Andrievskii et al. (126) report that the structure of films of In_2Se_3 and In_2Te_3 depends strongly on conditions of preparation. Rdf curves were obtained at temperatures from 20° to 70°C and appreciable changes in the curves were found. The tetrahedral coordination of In was considered to be preserved as in the crystalline form.

$\underline{Sb_2S_3}$

Rdf curves obtained by Tatarinova (147) using photographic electron diffraction show well-defined peaks but with considerable negative overshoot. The curves were interpreted in terms of a relatively close packed structure in which 5.7 S atoms surround an Sb atom and 3.8 Sb surround each S atom. In crystalline antimonite (148), the nearest neighboring distances extend from 2.33 to 2.67 Å with more atoms at distances between 2.84 and 3.60 Å. Reshetnikov (149) has also examined films of Sb_2S_3 obtaining a somewhat different rdf. It was concluded that the local order is similar to that of the antimonite crystal structure.

$\underline{Sb_2Se_3}$

Films were prepared by vapor deposition onto plastic film substrates at room temperature by Tatarinova (91). Rdfs were obtained with a well-defined peak at 2.45 Å. The second peak was considered to consist of a group of three closely spaced peaks at 3.30, 3.68 and 4.35 Å. The rdf shows considerable negative overshoot, however. In the crystalline phase the distance between Sb-Se atoms is 2.50 Å, while the distance between Sb-Sb and Se-Se neighbors is 2.72 and 2.82 Å, respectively; the structure consists of chains parallel to the c axis (150). In work by Andrievskii et al. (126), a nearest neighbor distance of 2.52 Å was obtained which increased with heat treatment to 2.63 Å. The nearest neighbor coordination number was found to be much lower than in the crystalline form.

$\underline{Sb_2Te_3}$

Films of Sb_2Te_3 prepared by Andrievskii et al. (126) were found to have a nearest neighbor distance of 2.78 Å, approximately the sum of the covalent radii of Sb and Te. In crystalline Sb_2Te_3, however, the shortest interatomic distances are 3.07, 3.17 and 3.63 Å between the atom pairs Sb-Te, Sb-Te and Te-Te, respectively (151). The structure of the films did not depend on thickness but changed slightly with heat treatment.

$\underline{SiO \text{ and } SiO_2}$

Films of SiO of varying Si to O ratio were prepared by Coleman and Thomas (152) using glow discharge techniques. SiO films were also prepared by evaporation in vacuum, and films of SiO_2 were blown from the bulk. Electron diffraction patterns were recorded electrically using a silicon solar cell as detector but inelastically scattered electrons were not experimentally eliminated. The rdfs of films of SiO_2 were found to be in agreement with previous x-ray work, for example by Zarzychi (153), but do not possess the resolution of later x-ray work by Warren and collaborators (34). The authors concluded that SiO films consist of a mixture of Si and SiO_2 as suggested by Brady from x-ray work (154) and by Lin and Joshi (155), who carried out x-ray examination of bulk samples. This result, however, has been questioned by Kaplow (156) in an x-ray re-evaluation and by Dove and Molnar using scanning electron diffraction on thin films (157).

Pavlov and Shitova (158) carried out electron diffraction examination of SiO_2 films using photographic techniques. The authors conclude that, regardless of the several conditions of

preparation employed, the films possessed an amorphous structure with short range order corresponding to the structure of β-cristobalite.

$\underline{Si_3N_4}$

Amorphous films prepared by a glow discharge technique could be varied in average composition from silicon to silicon nitride. Coleman and Thomas obtained electron diffraction patterns from these films using an electronic recording system but without an energy filter. The intensity curves show very small ripples about the mean scattering curve, possibly due to the inclusion of inelastically scattered electrons. The rdfs appear to be very diffuse but are interpreted by the authors as indicative that the films consisted of mixtures of silicon and Si_3N_4 (159).

T&Se

Thin films of T&Se were deposited, by Aliev and Tatarinova (160), onto room temperature rock salt and collodian substrates from bulk material heated in a tungsten spiral. The diffuse electron diffraction pattern was recorded photographically and the rdf calculated. An extremely broad first peak was obtained and was considered to consist of a number of overlapping peaks. The curve could not be reconciled with the local order present in the (tetragonal) crystal structure of T&Se, however (161), either in coordination numbers or nearest neighbor distance. The nearest neighbor distance indicated by the very broad first peak was 2.90 Å with coordination 2, while in the T&-Se crystalline form the nearest neighbor distance is 2.68 with coordination 4.

$CdGe_xAs_2$

In an x-ray study on bulk quenched material, Cervinka et al. (162) found that the rdfs could be interpreted in terms of the nearest neighbor order of crystalline $CdAs_2$. A detailed discussion is given of the crystal structure of CdAs and $CdGeAs_2$.

$CdGeP_2$

Grigorovici et al. examined bulk specimens using x-ray techniques (163). The first peak in the rdf was found to be consistent with overlapping peaks due to Cd-P and Ge-P contributions with bond lengths of 2.55 and 2.33 Å and coordination numbers as in the crystalline form. It is deduced that each P atom has two Cd and two Ge neighbors at somewhat different distances, as in the crystalline material.

Si and Ge Ternary Chalcogenides

Hilton and collaborators (164) have carried out some x-ray rdf measurements on bulk samples of chalcogenides as part of an extensive investigation of infrared optical glasses. Results are reported on the compositions $SiTe_4$, 15Si15As70Te, 15Si45As40Te, 30Si15As55Te and 15Ge45As40Te. It is concluded that where possible Si-Te, Si-As and As-Te bonds are formed in preference to Si-Si, As-As, Te-Te bonds. The results are of particular interest (although ripples are evident in the data at low values), since infrared and thermodynamic data are also reported.

Acknowledgements

The author is indebted to F. Betts, A. Bienenstock, J. Chang, B. C. Giersen, J. F. Graczyk, F. W. Lytle, B. Molnar, S. Moss, S. R. Ovshinski, D. E. Sayers, E. A. Stern and C. N. Wagner and their publishers for permission to reproduce figures.

The receipt of research support from the National Science Foundation and from ARO-Durham DAHC04-70-C-0024 is greatfully acknowledged.

List of References

1. L. H. Germer, Phys. Rev. 56, 58 (1939).

2. L. R. Maxwell and V. M. Mosely, Phys. Rev. 47, 330 (1935).

3. B. E. Warren, H. Krutter and O. Morningstar, J. Amer. Ceram. Soc. 19, 202 (1936).

4. K. L. Chopra, "Thin Film Phenomena," McGraw-Hill, New York, 1969.

5. Handbook of Thin Film Technology (L. I. Maissel and R. Glang, eds.), McGraw-Hill, New York, 1970.

6. P. Debye, Ann. Physik 46, 809 (1915).

7. F. Zernike and J. A. Prins, Z. Physik 41, 184 (1927).

8. P. Debye and H. Menke, Ergeb d. Tech Rontgenk. 2, 1 (1931).

9. R. Hosemann and S. N. Bagghi, "Direct Analysis of Diffraction by Matter," North Holland Publ. Co., Amsterdam, 1962.

10. A. Guinier, "X-ray Diffraction in Crystals, Imperfect Crystals and Amorphous Bodies," W. H. Freeman and Co., San Francisco, 1963.

11. B. E. Warren, "X-ray Diffraction," Addison-Wesley,Reading, 1969.

12. N. S. Gingrich, Rev. Mod. Phys. 15, 90 (1943).

13. K. Furukawa, Rep. Prog. Phys. , 396 (1963).

14. R. Grigorovici, J. Non-Crystalline Solids 1, 303 (1969).

15. Int'l. Conf. on Amorphous and Liquid Semiconductors, 1-4, published as special issues of the J. Non-Crystalline Solids.

16. "Non-Crystalline Solids" (V. D. Frechette, ed.), Wiley, New York, 1960.

17. C. J. Pings and J. Waser, J. Chem. Phys. 48, 3016 (1968).

18. I. N. Sneddon, "Fourier Transforms," McGraw-Hill, New York, 1951.

19. D. T. Keating, J. Appl. Phys. 34, 923 (1963).

20. D. B. Dove and P. N. Denbigh, Proc. Int'l. Congress of Electron Microscopy, p. 67, Kyoto, 1966.

21. L. H. Germer and A. H. White, Phys. Rev. 60, 447 (1941).

22. C. W. B. Grigson and G. Barton, Brit. J. Appl. Phys. 18, 175 (1967).

23. C. Morozumi and H. L. Ritter, Acta. Cryst. 6, 588 (1953).

24. V. H. Tsiensuu, S. Ergun and L. Alexander, J. Appl. Phys. 35, 1718 (1961).

25. M. B. Heritage and P. I. Tillett, Proc. 7th Int'l Congress of Electron Microscopy, Grenoble, 1970.

26. Y. Fukaro and C. M. Wayman, J. Appl. Phys. 40, 1656 (1964).

27. S. C. Moss and J. F. Graczyk, Phys. Rev. Letters 23, 1167 (1969).

28. P. N. Denbigh and D. B. Dove, J. Appl. Phys. 38, 99 (1967).

29. C. S. Cargill, J. Appl. Cryst., to appear.

30. H. Richter and A. Rukwied, Z. Physik 160, 473 (1960).

31. J. Gjonnes, Acta Cryst. 12, 976 (1959).

32. H. Morimoto, J. Phys. Soc. Japan 13, 1015 (1958).

33. H. Seip, in "Selected Topics in Structural Chemistry" (P. Andersen, O. Bastiansen and S. Furberg, eds.), p. 26, Scandinavian University Books, Oslo, 1967.

34. R. L. Mozzi and B. E. Warren, J. Appl. Cryst. 2, 164 (1969).

35. L. S. Bartell and L. O. Brockway, J. Appl. Phys. 24, 656 (1953).

36. J. M. Cowley, Acta Cryst. 6, 516 (1953).

37. C. W. B. Grigson, J. Electronics and Control 12, 207 (1962).

38. C. W. B. Grigson, Rev. Sci. Instr. 36, 1587 (1965).

39. D. B. Dove and P. N. Denbigh, Rev. Sci. Instr. 37, 1687 (1966).

40. C. W. B. Grigson, Advances in Electronics and Electron Physics, Suppl. 4, p. 187, Academic Press, 1968.

41. G. Molensteht, Optik 5, 449 (1952); 9, 473 (1952).

42. H. Boersch, Z. Physik 139, 115 (1954).

43. J. A. Simpson and L. Marton, Rev. Sci. Instr. 32, 802 (1961).

44. C. Burggraf and S. Goldsztaub, J. de Microscopie 1, 441 (1962).

45. H. Raether, Springer Tracts in Modern Physics, Vol. 38, p. 84, 1965.

46. J. F. Graczyk and S. C. Moss, Rev. Sci. Instr. 40, 424 (1969).

47. Vacuum Generators, Ltd., marketed by Veeco Vacuum Corp.

48. A.E.I. Scientific Apparatus, Ltd., Harlow, England.

49. W. Buckel, Z. Physik 138, 136 (1954).

50. W. Buckel and R. Hilsch, Z. Physik 138, 109 (1954).

51. H. Bulow and W. Buckel, Z. Physik 145, 141 (1956).

52. A. I. Bublick and B. Ia. Pines, Doklady 87, 215 (1952).

53. For a review see K. Berhndt, J. Vac. Sci. Techn. 7, 385 (1970).

54. S. Fujime, Japan J. Appl. Phys. 5, 1029 (1966).

55. S. Fujime, Japan J. Appl. Phys. 6, 305 (1967).

56. C. W. B. Grigson, D. B. Dove and G. R. Stilwell, Nature 204, 173 (1964).

57. W. A. Jesser and J. W. Matthews, Phil. Mag. 15, 1097 (1967).

58. L. Kaufman, E. V. Clougherty and R. J. Weiss, Acta Met. 11, 323 (1963).

59. L. D. Blackburn, L. Kaufman and M. Cohen, Acta Met. 13, 533 (1965).

60. C. N. J. Wagner, J. Vac. Sci. Techn. 6, 650 (1969); N. Giessen and C. N. J. Wagner, Liquid Metals, Chemistry and Physics, Marcel Dekker, New York, 1972.

61. S. Geiling and H. Richter, Acta Cryst. 2, 305 (1949).

62. H. Richter and G. Gommel, Z. Naturforschung 12a, 996 (1957).

63. G. Breitling, J. Vac. Sci. Techn. 6, 628 (1969).

64. H. Richter and G. Breitling, Z. Naturforschung 6a, 721 (1951).

65. H. Krebs and R. Steffen, Z. Anorg. Allgemeine Chemie 327, 224 (1964).

66. L. S. Palatnik and V. M. Kosevich, Sov. Phys. Cryst. 3, 716 (1958); 4, 37 (1959); 4, 633 (1959).

67. R. Leonhardt, H. Richter and W. Rossteutscher, Z. Physik 165, 121 (1961).

68. H. Richter, Z. Physik 172, 530 (1963).

69. H. Richter and G. Breitling, Z. Physik 21a, 1710 (1966).

70. S. Fujime, Japan J. Appl. Phys. 5, 59 (1966); 5, 764 (1966).

71. M. Takagi, J. Phys. Soc. Japan 11, 396 (1956).

72. S. Fujime, Japan J. Appl. Phys. 5, 778 (1966).

73. K. Katada, Japan J. Appl. Phys. 5, 582 (1966).

74. J. Kakinoki, K. Katada, T. Hanawa and T. Ino, Acta Cryst. 13, 171 (1960).

75. B. T. Boiko, L. S. Palatnik and A. S. Derevyanchenko, Sov. Phys. Doklady 13, 237 (1968).

76. B. T. Boiko, L. S. Palatnik, A. S. Derevyanchenko and Yu M. Voronin, Sov. Phys. Solid State 10, 520 (1968).

77. D. B. Dove, Proc. 26th Annual Meeting EMSA, 396 (1968).

78. M. B. Heritage, D. B. Dove and P. N. Denbigh, to be published.

79. T. Noda and M. Inagaki, Bull. Chem. Soc. Japan 37, 534 (1964).

80. K. Furukawa, Nihon Kessho Gakkaishi 6, 101 (1964).

81. R. D. Heidenreich, B.S.T.J. XLV, 651 (1966).

82. F. P. Bundy and J. S. Kasper, J. Chem. Phys. 46, 3437 (1967).

83. M. L. Rudee, Carbon 5, 155 (1967).

84. H. Konig, Optik 3, 301 (1948).

85. H. Richter and O. Furst, Z. Naturforschung 6a, 38 (1951).

86. H. Richter and G. Breitling, Z. Naturforschung 13a, 988 (1958).

87. R. Grigorovici and R. Manaila, Thin Solid Films 1, 343 (1968).

88. R. Grigorovici, R. Manaila and A. A. Vaipolin, Acta Cryst. B24, 535 (1968).

89. F. Herre and H. Richter, Z. Physik 150, 149 (1958).

90. H. Richter and U. Steele, Naturwissenschaften 45, 461 (1958); Z. Metallkunde 50, 369 (1959).

91. L. I. Tatarinova, Sov. Phys. Cryst. 4, 637 (1959).

92. M. V. Coleman and D. J. D. Thomas, Phys. Stat. Solidi 24, K111 (1967).

93. J. Chang and D. B. Dove, Proc. 7th Int'l Conf. on Electron Microscopy, p. 183, Grenoble, 1970.

94. "Physics of Electronic Ceramics" (L. L. Hench and D. B. Dove, eds.), p. 260, Marcel Dekker, New York, 1971.

95. D. E. Polk, J. Non-Crystalline Solids 5, 365 (1970).

96. D. Henderson and F. Herman, 4th Int'l Conf. on Amorphous and Liquid Semiconductors, Ann Arbor, Mich., 1971.

97. N. J. Shevchik, 4th Int'l Conf. on Amorphous and Liquid Semiconductors, Ann Arbor, 1971.

98. M. H. Brodsky and R. S. Title, Phys. Rev. Letters 23, 581 (1969).

99. M. L. Rudee, Physica Status Solidi 646, K1 (1971).

100. D. E. Sayers, E. A. Stern and F. W. Lytle, Phys. Rev. Letters, to be published.

101. H. Krebs and F. Schultze-Gebhardt, Acta Cryst. 8, 412 (1955).

102. H. Keller and J. Stuke, Phys. Status Solidi 8, 831 (1965).

103. H. Hendus, Z. Physik 119, 265 (1942).

104. H. Richter, W. Kulcke and H. Specht, Z. Naturforschung 7a, 511 (1952).

105. H. Richter and G. Breitling, Rev. Int. Hautes Tempér et Refract. 4, 213 (1967).

106. H. Richter and F. Herre, Z. Naturforschung 13a, 874 (1958).

107. H. Richter, Z. Naturforschung 13, 32 (1958).

108. E. H. Grimminger, H. Gruninger and H. Richter, Naturwiss 42, 256 (1955).

109. E. H. Henninger, R. C. Buschert and L. Heaton, J. Chem. Phys. 46, 586 (1967).

110. R. Kaplow, T. A. Rowe and B. L. Averbach, Phys. Rev. 168, 1068 (1968).

111. G. Lucovsky, Matl. Res. Bull. 4, 505 (1969).

112. G. Lucovsky, "Physics of Selenium and Tellurium" (W. C. Cooper, ed.), p. 255, Pergamon Press, 1969.

113. A. I. Andrievskii, E. D. Nabitovich and Ya. V. Voloshchuk, Sov. Phys. Cryst. 5, 349 (1960).

114. S. Mader, J. Vac. Sci. Techn. 2, 35 (1965).

115. P. Duwez and R. H. Willens, Trans. Met. Soc. AIME 227, 362 (1962).

116. S. Fujime, Japan J. Appl. Phys. 5, 643 (1966).

117. C. N. J. Wagner, T. B. Light, N. C. Halder and W. E. Lukens, J. Appl. Phys. 39, 3690 (1968).

118. T. B. Light and C. N. J. Wagner, J. Appl. Cryst. 1, 199 (1968).

119. S. Fujime, Japan J. Appl. Phys. 5, 739 (1966).

120. R. W. Bicknell, Brit. J. Appl. Phys. 17, 775 (1966).

121. P. C. Sharah and G. P. Smith, J. Chem. Phys. 21, 228 (1953).

122. Structure Reports 12, 175 (1949).

123. A. I. Andrievskii, I. D. Nabitovich and Ya. V. Voloshchuk, Sov. Phys. Cryst. 6, 534 (1962).

124. A. G. Mikolaichuk and Ya. V. Dutchak, Sov. Phys. Cryst. 9, 86 (1969).

125. L. I. Tatarinova, Sov. Phys. Cryst. 1, 423 (1959).

126. A. I. Andrievskii, E. D. Nabitovich and Ya. V. Dutchak, Sov. Phys. Cryst. 7, 704 (1963).

127. R. W. Fawcett, C. N. J. Wagner and G. S. Cargill, J. Non-Crystalline Solids 8-10, 369 (1972).

128. B. Molnar and D. B. Dove, to be published.

129. L. Ch'un-hua, A. S. Pashinkin and A. V. Novoselova, Russ. J. Inorg. Chem. 7, 1117 (1962).

130. L. Ross and M. Bourgon, Can. J. Chem. 47, 2555 (1969).

131. A. G. Mikolaichuk and A. N. Kolgut, Sov. Phys. Cryst. 15, 294 (1970).

132. B. J. Molnar, M.S. Thesis, University of Florida, 1971.

133. D. E. Sayers, F. W. Lytle and R. A. Stern, J. Non-Crystalline Solids, 8-10, 401 (1972).

134. A. Bienenstock, F. Betts and S. R. Ovshinsky, J. Non-Crystalline Solids 2, 347 (1970).

135. F. Betts, A. Bienenstock and S. R. Ovshinsky, J. Non-Crystalline Solids 4, 554 (1970).

136. P. Duwez, Trans. ASM 60, 607 (1967).

137. D. B. Dove, M. B. Heritage, K. L. Chopra and S. K. Bahl, Appl. Phys. Letters 16, 138 (1970).

138. J. Goldak, C. S. Barrett, D. Innes and W. Youdelis, J. Chem. Phys. 44, 3323 (1966).

139. D. B. Dove, J. Chang and B. Molnar, J. Non-Crystalline Solids 8-10, 377 (1972).

140. A. R. Hilton, C. E. Jones and M. Brau, Phys. Chem. Glasses 7, 105 (1966).

141. D. Adler, M. H. Cohen, E. A. Fagen and J. C. Thompson, J. Non-Crystalline Solids 3, 402 (1970).

142. F. Betts, A. I. Bienenstock and C. W. Bates, J. Non-Crystalline Solids 8-10, 364 (1972).

143. T. Takemori, R. Roy and G. T. McCarthy, Matl. Res. Bull. 5, 529 (1970).

144. L. I. Tatarinova, Sov. Phys. Cryst. 15, 742 (1971).

145. L. I. Tatarinova and T. S. Kagmazovskaya, Sov. Phys. Cryst. 6, 538 (1962).

146. S. A. Semiletov, Sov. Phys. Cryst. 3, 292 (1958).

147. L. I. Tatarinova, Sov. Phys. Cryst. 2, 251 (1957).

148. Sturcturbericht, Vol. III, p. 49.

149. A. M. Reshetnikov, Sov. Phys. Cryst. 4, 883 (1959).

150. N. W. Tideswell, F. H. Kruse and J. D. McCullough, Acta Cryst. 10, 99 (1957).

151. S. A. Semiletov, Sov. Phys. Cryst. 1, 317 (1956).

152. M. V. Coleman and D. J. D. Thomas, Phys. Status Solidi 22, 593 (1967).

153. J. Zarzychi, Verres et Refract. 11, 3 (1957).

154. G. W. Brady, J. Chem. Phys. 63, 1119 (1959).

155. S. C. H. Lin and M. Joshi, J. Electrochem. Soc. 116, 1740 (1969).

156. R. Kaplow, J. Appl. Phys. 43, 995 (1972).

157. B. Molnar and D. B. Dove, J. Amer. Ceram. Soc., to be published.

158. P. V. Pavlov and E. V. Shitova, Sov. Phys. Cryst. 6, 538 (1962).

159. M. V. Coleman and D. J. D. Thomas, Phys. Status Solidi 25, 241 (1968).

160. F. I. Aliev and L. I. Tatarinova, Sov. Phys. Cryst. 11, 349 (1966).

161. J. Katelaar, W. t'Hart, M. Moerel and D. Polder, Z. Kristallogr. 101, 396 (1939).

162. L. Cervinka, R. Hosemann and W. Vogel, J. Non-Crystalline Solids 3, 294 (1970).

163. R. Grigorovici, R. Manaila and A. M. Vaipolin, Acta Cryst. B24, 535 (1968).

164. A. R. Hilton, C. E. Jones, R. D. Dobrott, H. M. Klein, A. M. Bryant and T. D. George, Phys. Chem. Glasses 7, 117 (1966).

List of Figure Captions

Fig. 1. a) Theoretical rdf of an array of isolated randomly oriented cubes of the diamond structure. The atoms are assumed to possess a small thermal vibrational amplitude.

b) Rdf curve obtained by transforming the theoretical si(s) curve over the range 0 to 1.95.

c) Result of transforming si(s)exp(- s^2) over the range 0 to 1.95. Comparison with the true rdf of 1(a) shows the degree of peak broadening introduced by the use of a termination function and a finite range in s.

Fig. 2. Calculated intensity curves, plotted as in (intensity), for arrays of small fcc crystallites are compared with the experimental result for a 10 Å deposit of Ni.

Fig. 3. a) The rdf calculated from one of the theoretical intensity curves of Fig. 2.

b) The rdf calculated from the experimental curve for the 10 Å deposit of Ni.

Fig. 4. Mean nearest neighbor atomic coordination number calculated for cubic fcc crystallites.

Fig. 5. Schematic diagram of a scanning electron diffraction system. See Ref. 40 for a comprehensive review of the direct recording technique.

Fig. 6. A series of rdfs obtained for very thin lead deposits by Heritage and Tillett (25). The results show direct evidence for close-packed non-fcc clustering at the

earliest stages of growth, prior to the development of fcc crystallites.

Fig. 7. The full curve shows the rdf of amorphous iron films, the dashed curve shows the x-ray results on splat cooled Fe-P-C foils obtained by Wagner (60a).

Fig. 8. Curves of $4\pi r[\rho(r)-\rho_o]$ for liquid Fe and for Fe-P-C foils obtained by x-rays, from a review by Giersen and Wagner (60b).

Fig. 9. Difference rdf curve of vapor deposited carbon film showing in this case a sequence of peaks consistent with graphitic local order. The minor ripples below 1 Å arise from the numerical Fourier transform procedure.

Fig. 10. Rdf of a silicon film obtained by Moss and Graczyk (27) using an electron microscope fitted with an energy filter and a direct intensity measurement system.

Fig. 11. Rdf of a germanium film obtained by scanning electron diffraction; (a) calculated without a terminating function showing ripples at small r and on both sides of the first peak, and (b) after deconvolution to remove termination ripple and peak broadening.

Fig. 12. Typical intensity curve for a $GeSe_{2.4}$ film obtained by Molnar (132). The breaks in the curve at s = 0.5 and 1.0 are due to electronic gain changes in the recording system. Inelastic background has been removed experimentally.

Fig. 13. Curve (a) shows the rdf for $GeSe_{2.4}$ obtained from the intensity data of Fig. 12. Curves (b) and (c) show the rdfs calculated from intensity curves obtained after successive heat treatment of the film.

Fig. 14. Atomic distribution curves for Se and Ge about Ge atoms and about Se atoms in $GeSe_2$. Results obtained by Lytle and collaborators (100) using x-ray absorption edge data.

Fig. 15. X-ray intensity curve of Ge_xTe_{1-x} films reported by Bienenstock and collaborators (134).

Fig. 16. Rdfs from the data of Fig. 15 showing a local order unlike that expected for a rock salt GeTe type of coordination, reported by Bienenstock and collaborators (134).

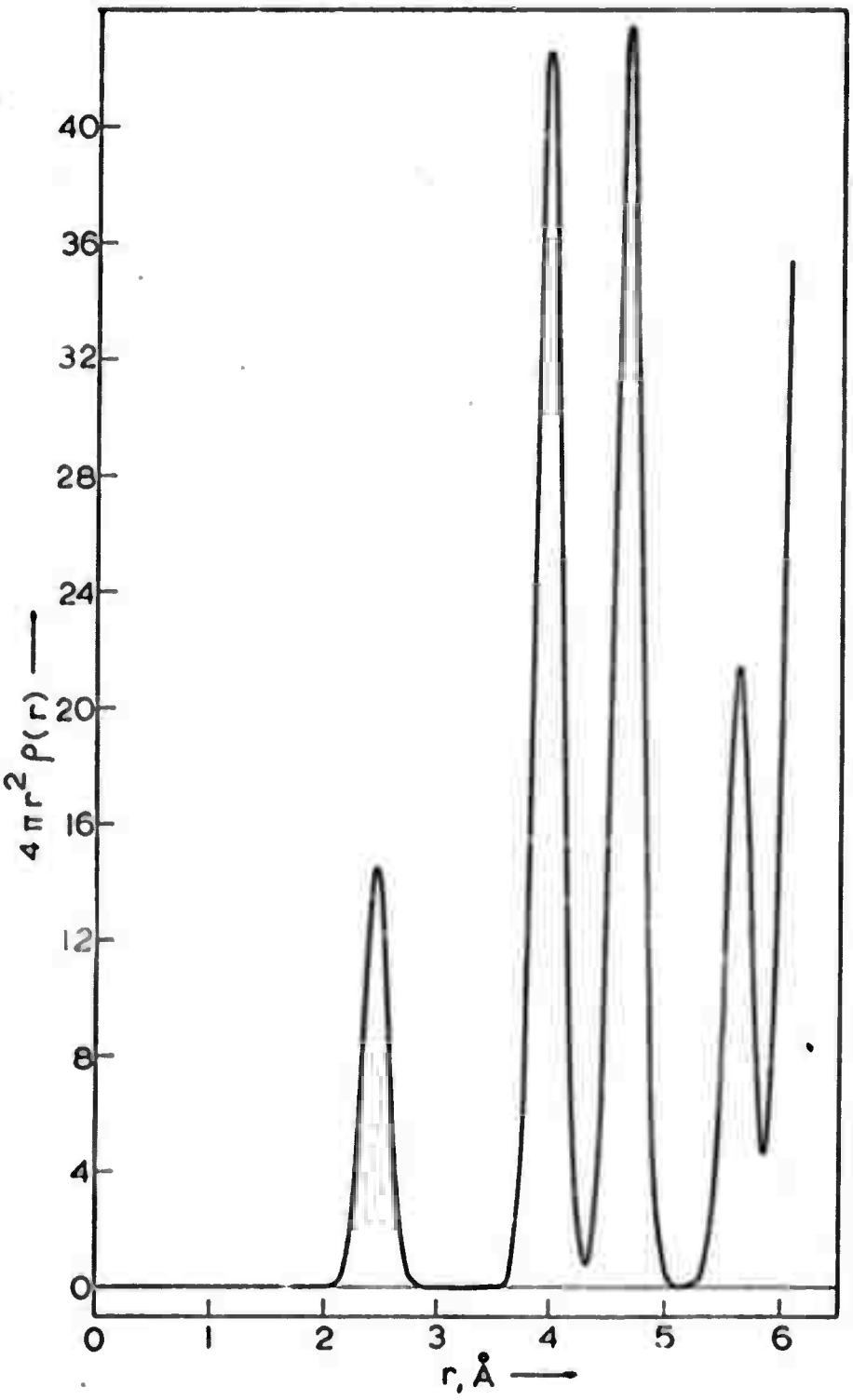

Fig. 1(a)

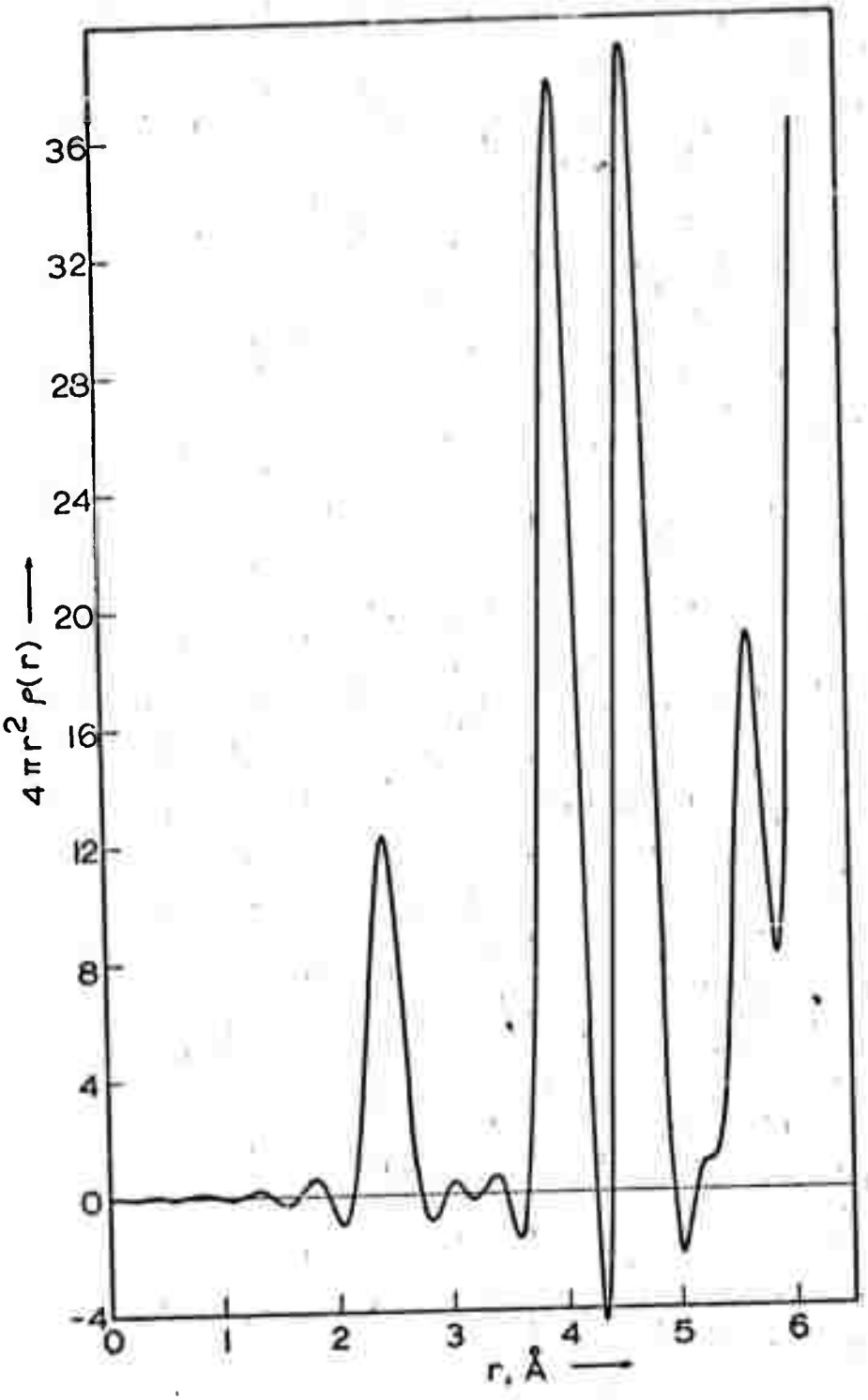

Fig. 1(b)

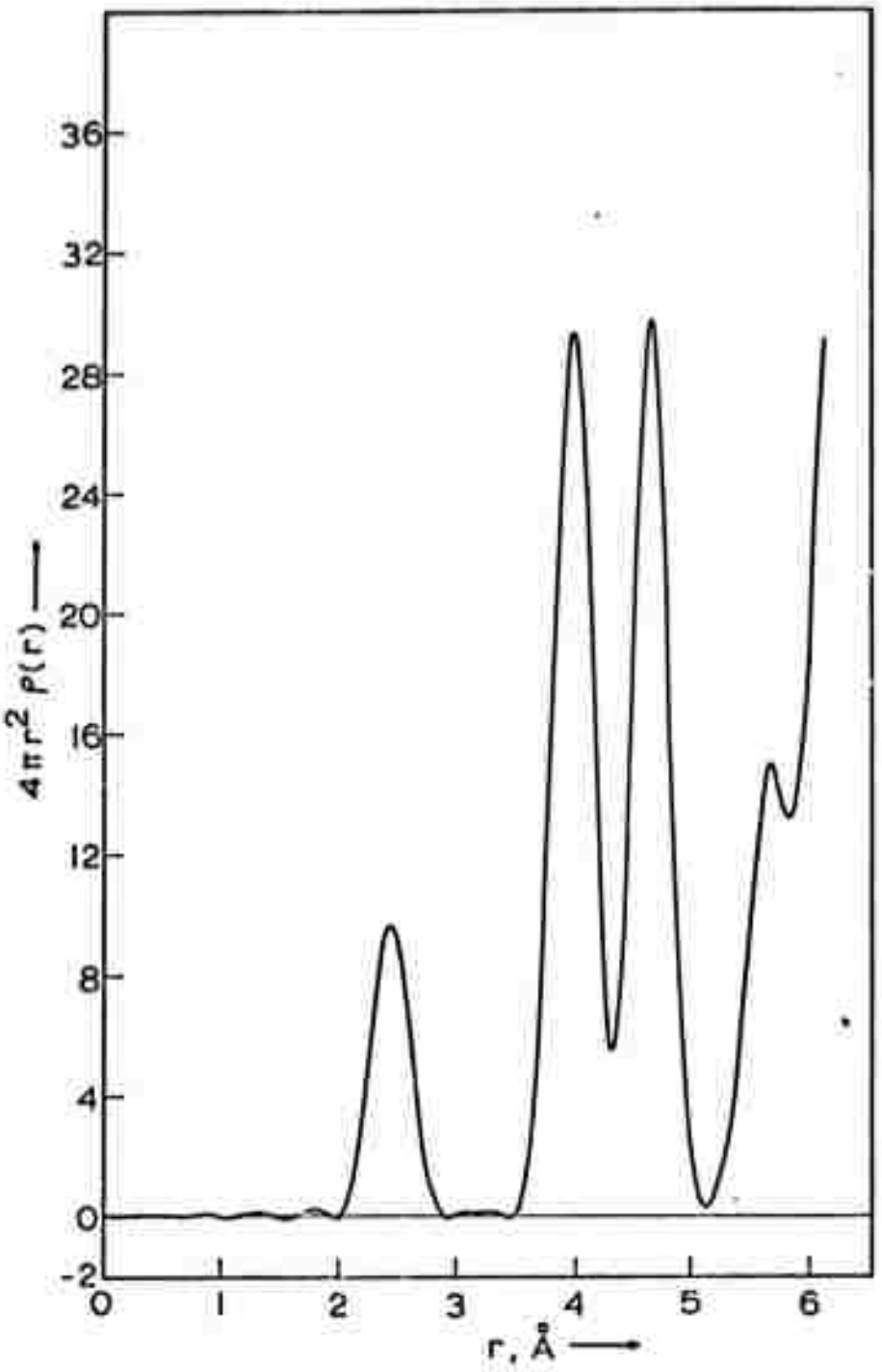

Fig. 1(c)

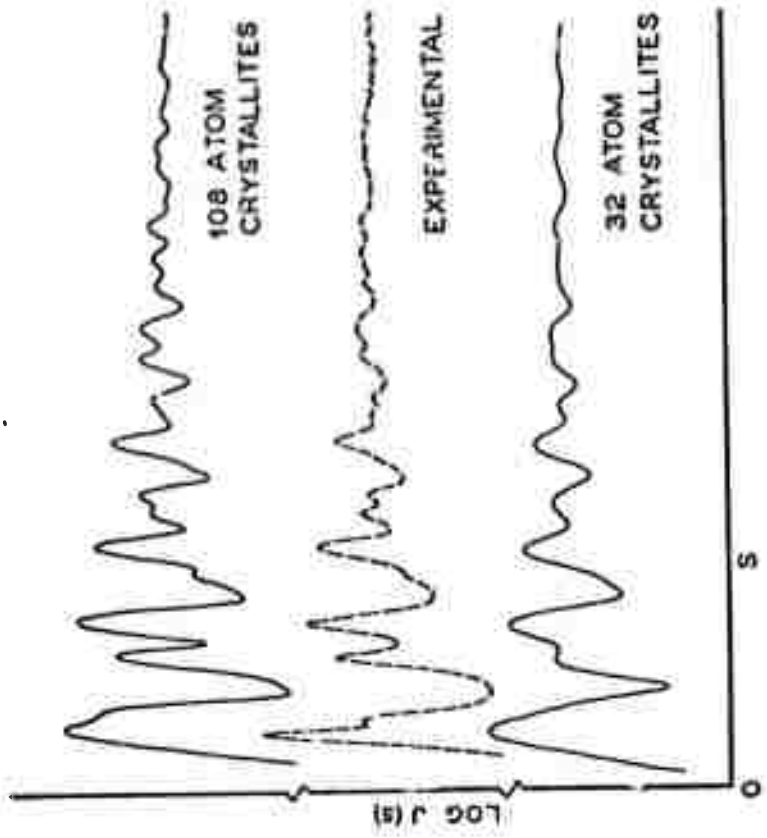
108 ATOM
CRYSTALLITES
EXPERIMENTAL
32 ATOM
CRYSTALLITES
S
0

Fig. 2.

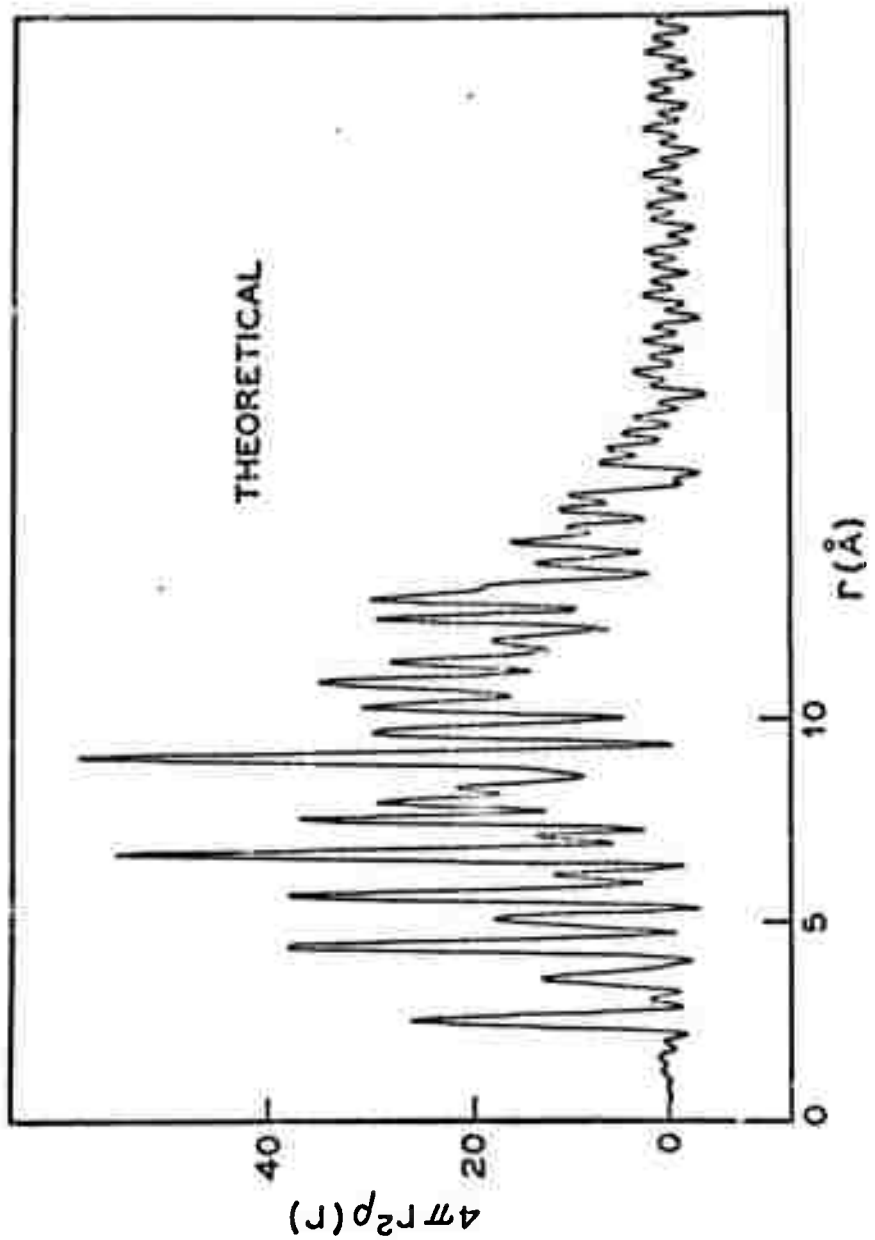

Fig. 3(a)

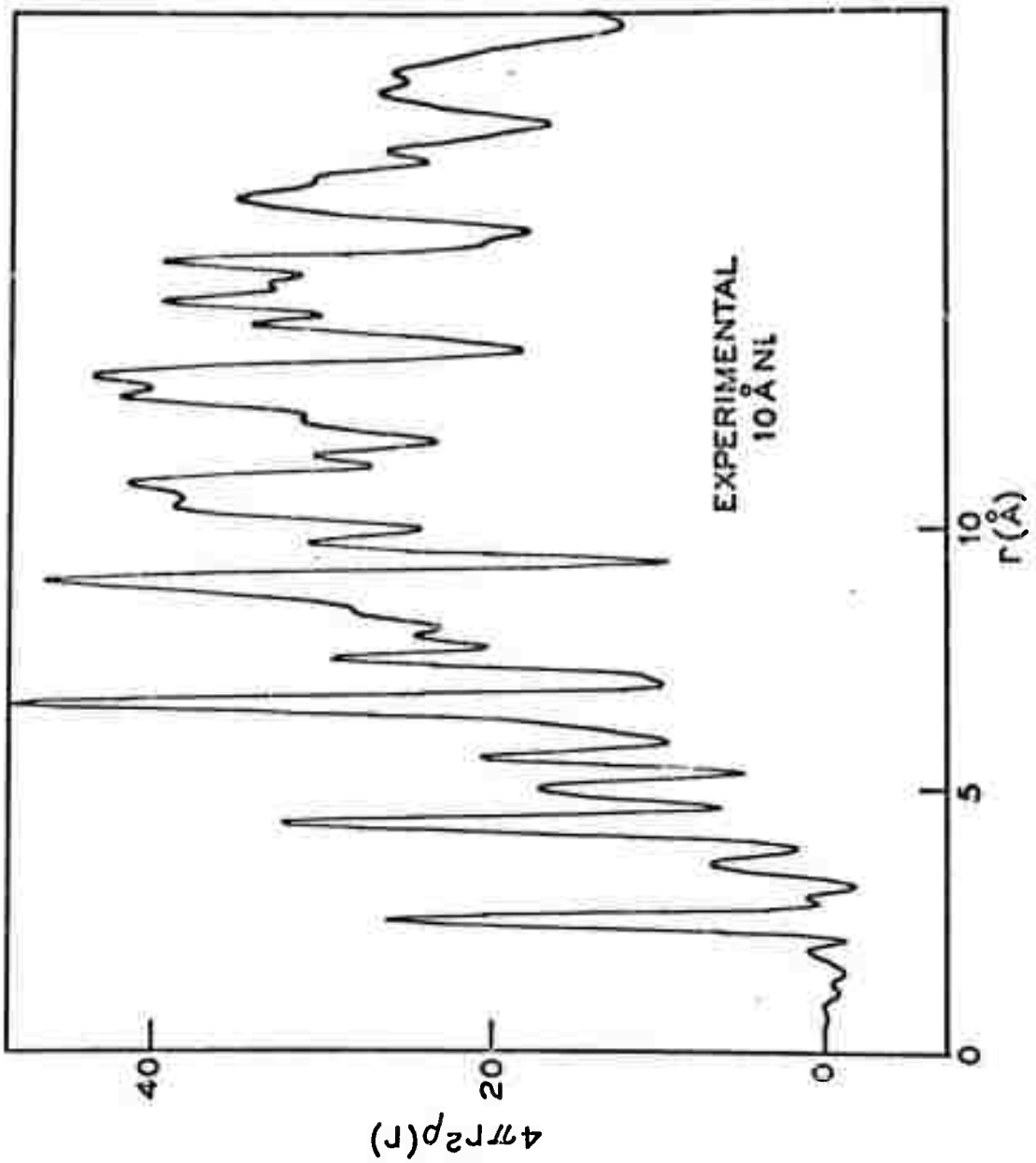

Fig. 3(b)

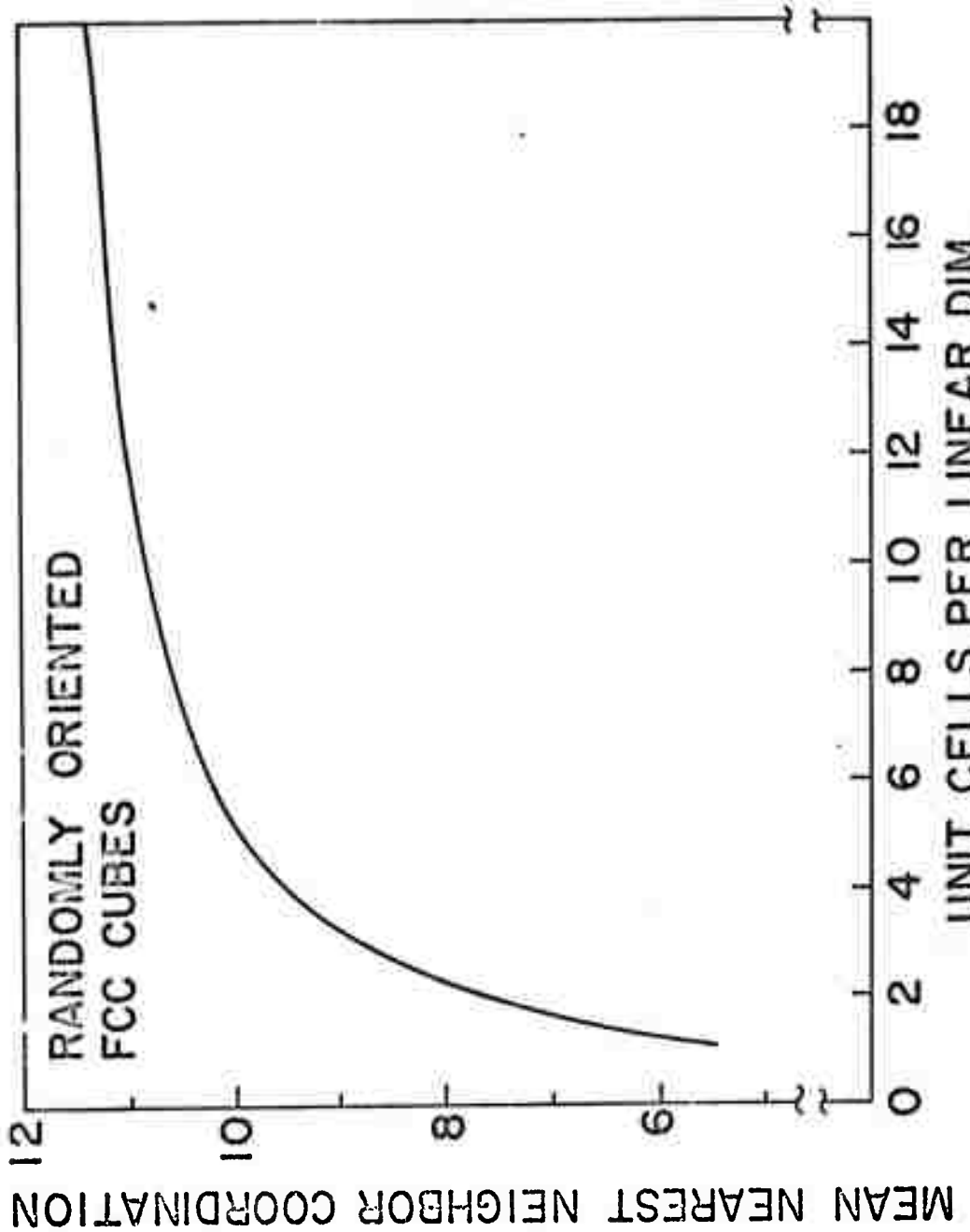
RANDOMLY ORIENTED
FCC CUBES
MEAN NEAREST NEIGHBOR COORDINATION
12
10
8
6
0
2
4
6
8
10
12
14
16
18
UNIT CELLS PER LINEAR DIM.

Fig. 4.

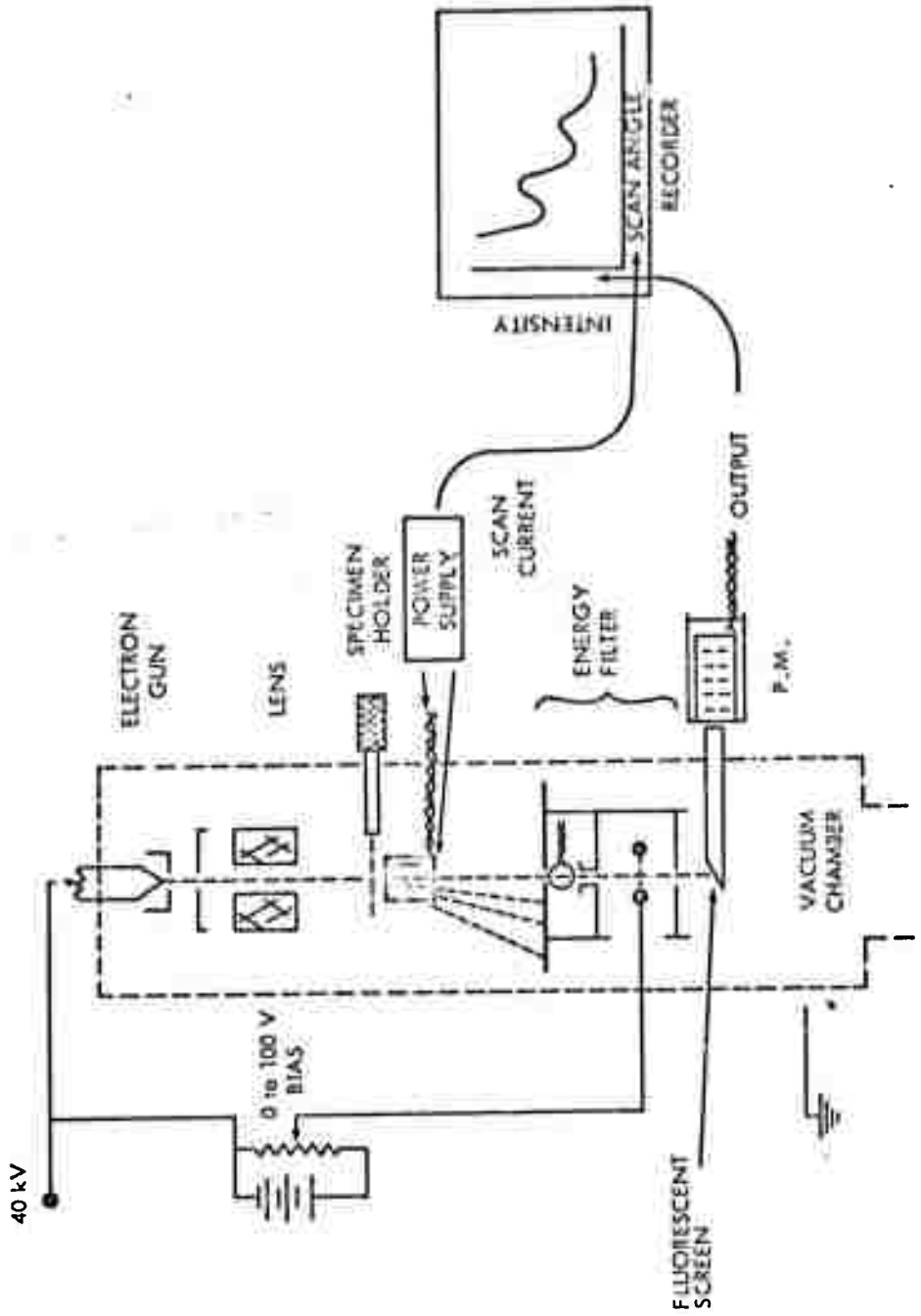
ELECTRON GUN
LENS
SPECIMEN HOLDER
POWER SUPPLY
SCAN CURRENT
ENERGY FILTER
OUTPUT
P.M.
INTENSITY
SCAN ANGLE
RECORDER
VACUUM CHAMBER
40 kV
0 to 100 V BIAS
FLUORESCENT SCREEN

Fig. 5.

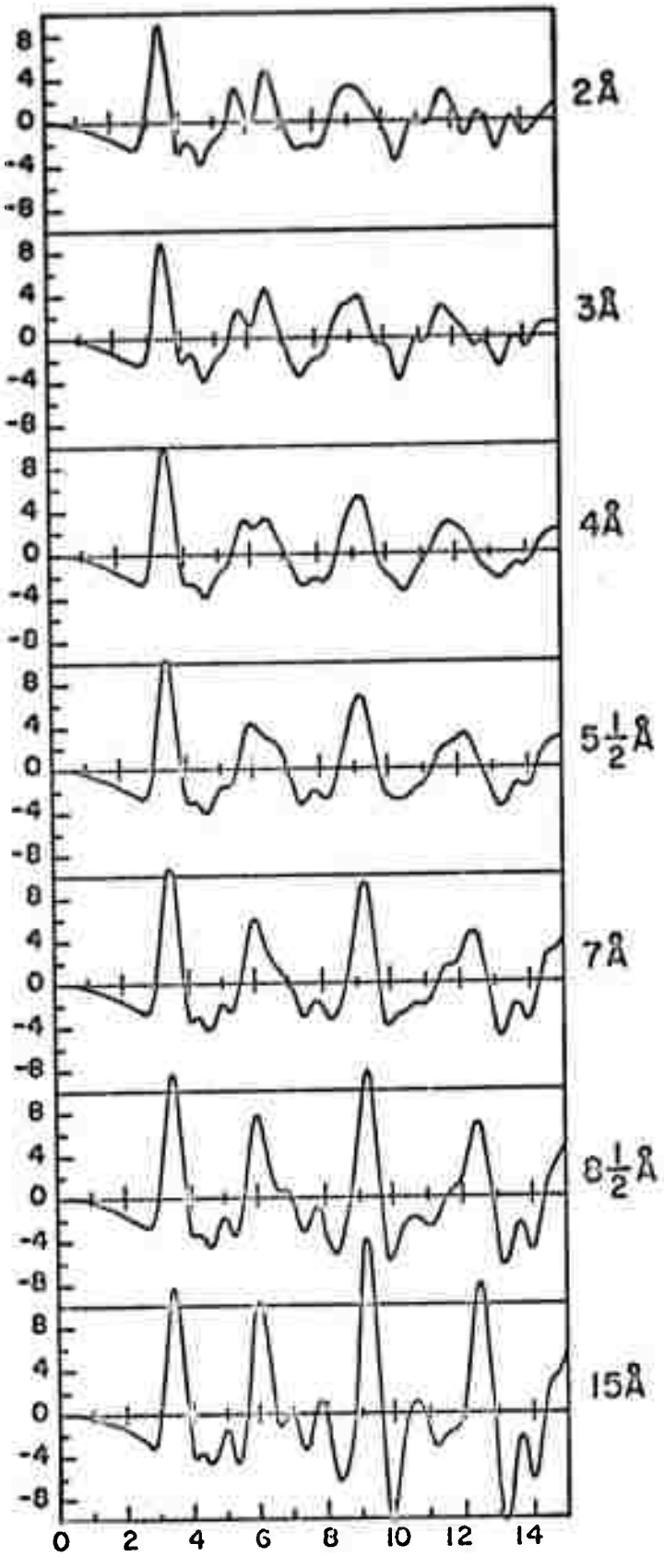

Fig. 6.

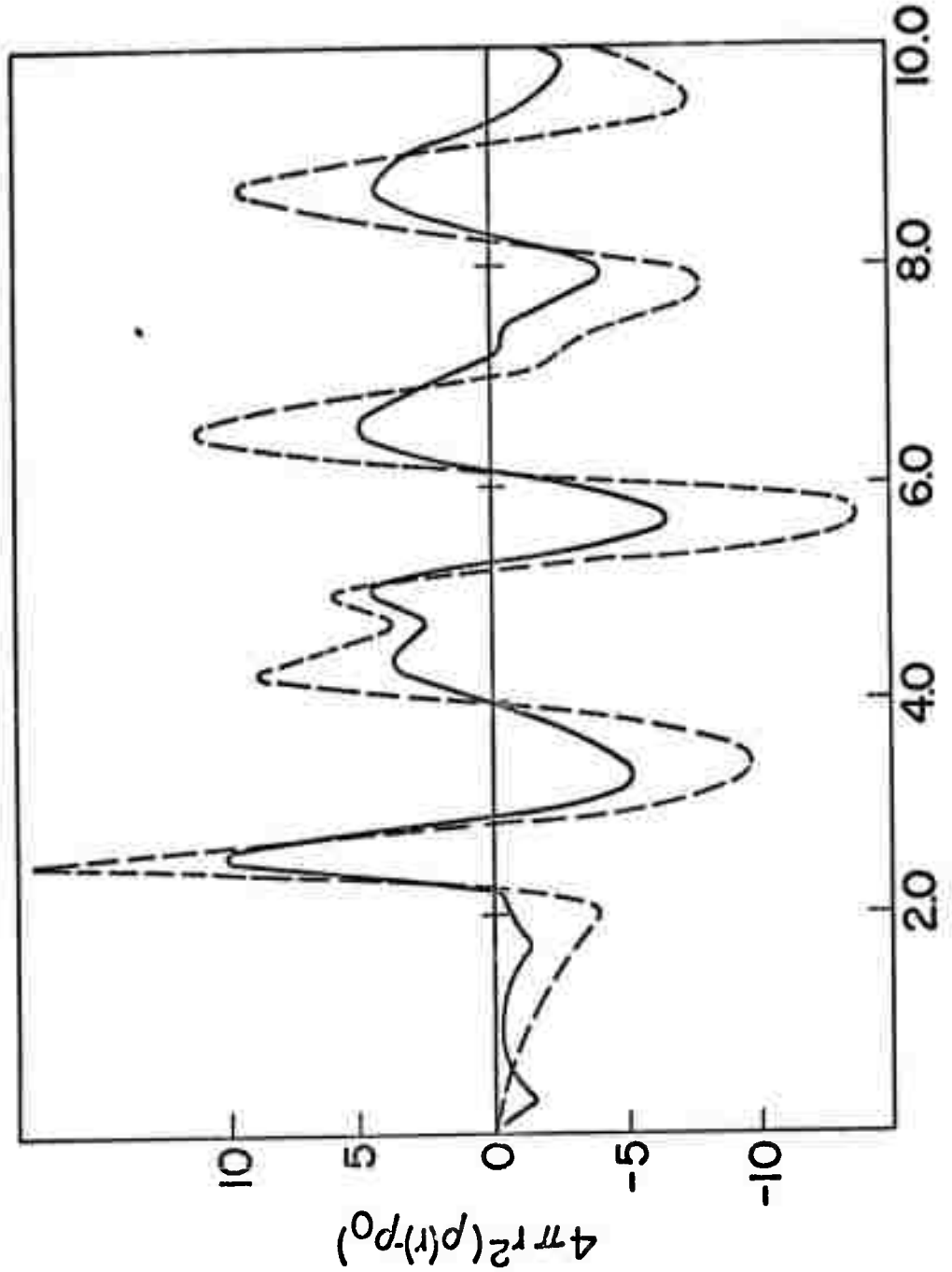

Fig. 7.

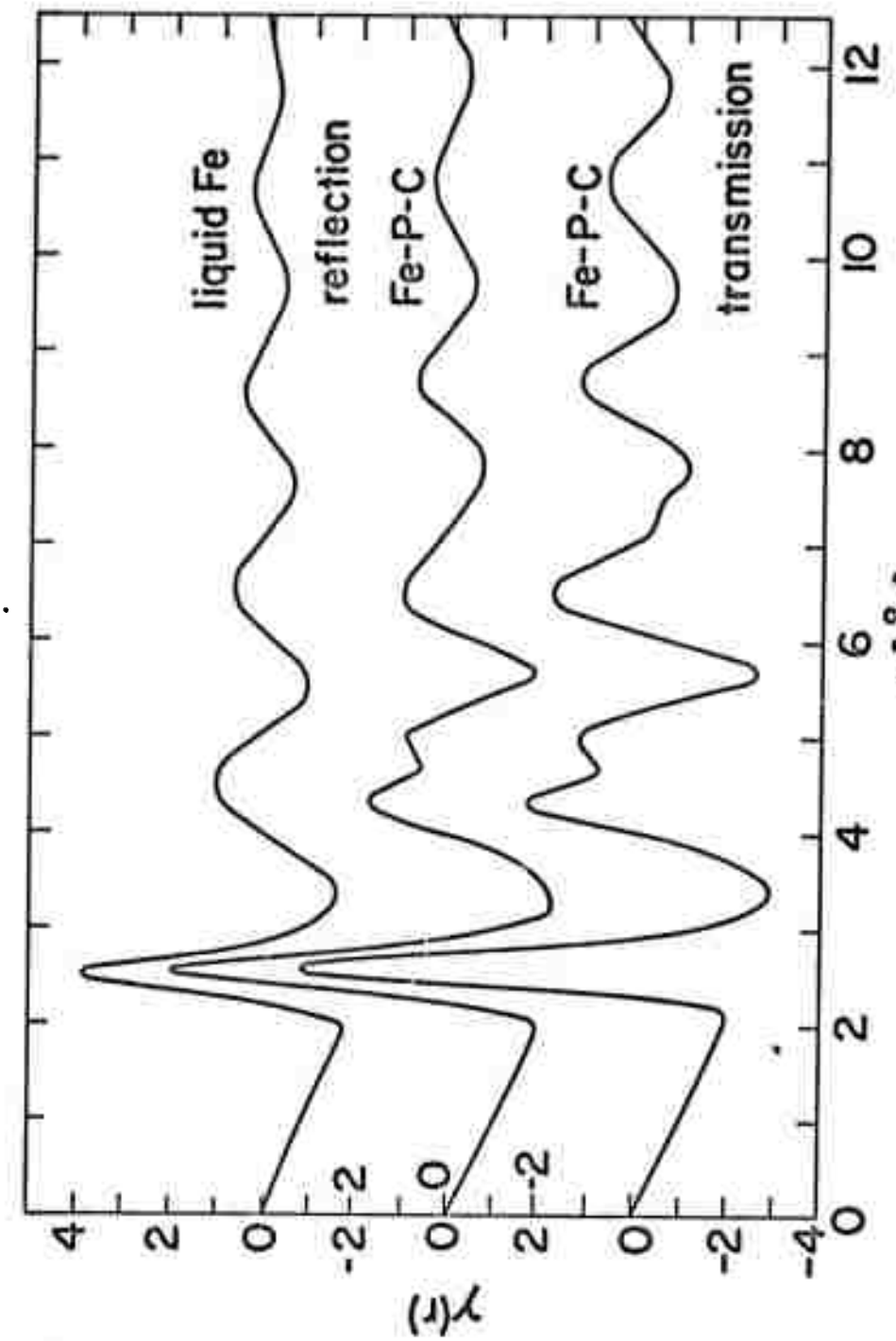
liquid Fe
reflection
Fe-P-C
Fe-P-C
transmission
γ(r)
r [Å]
4
2
0
-2
0
-2
2
0
-2
-4
0
2
4
6
8
10
12

Fig. 8.

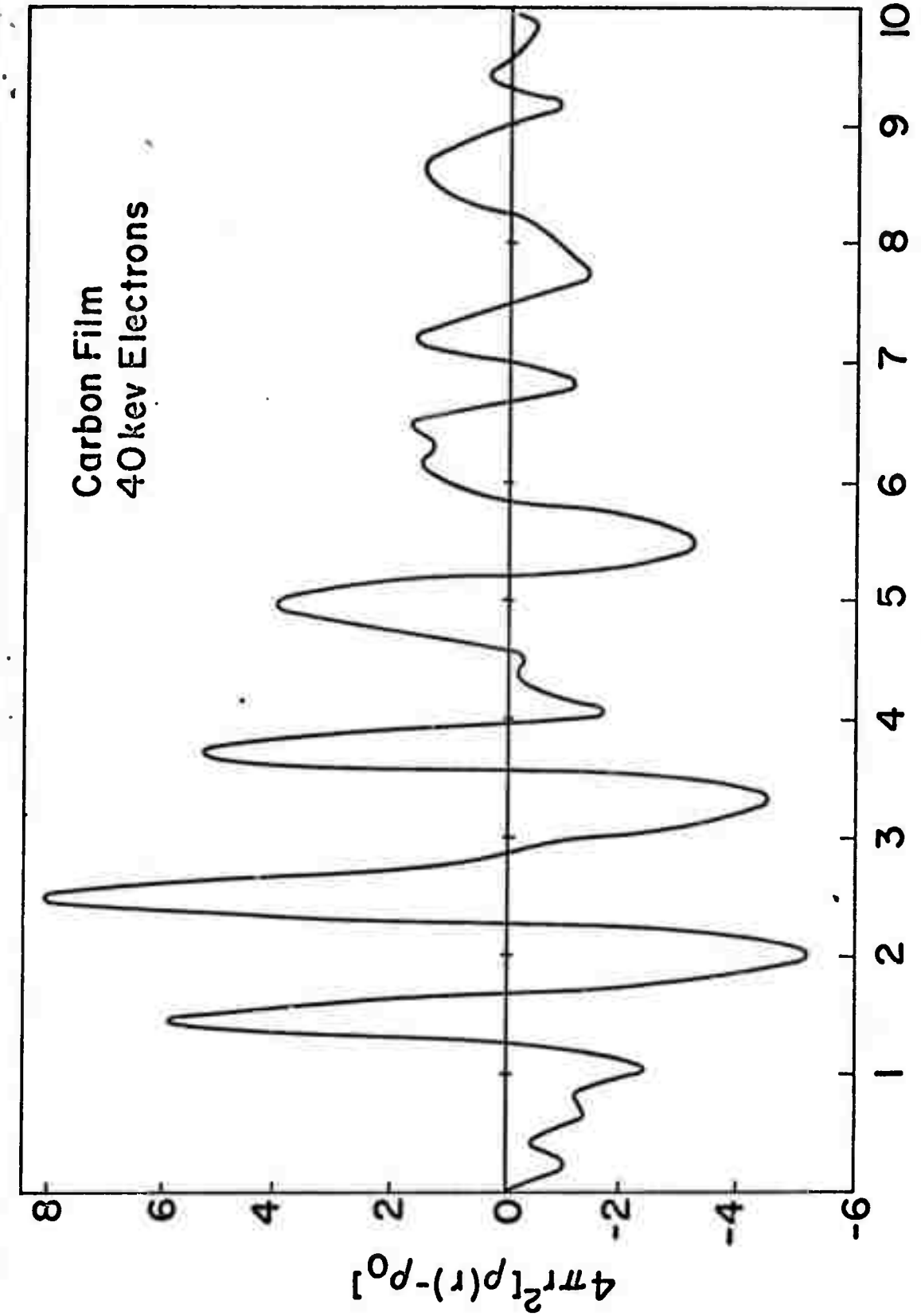
Carbon Film
40 kev Electrons
$4\pi r^2[\rho(r)-\rho_o]$
8
6
4
2
0
-2
-4
-6
1
2
3
4
5
6
7
8
9
10
r_s(Å)

Fig. 9.

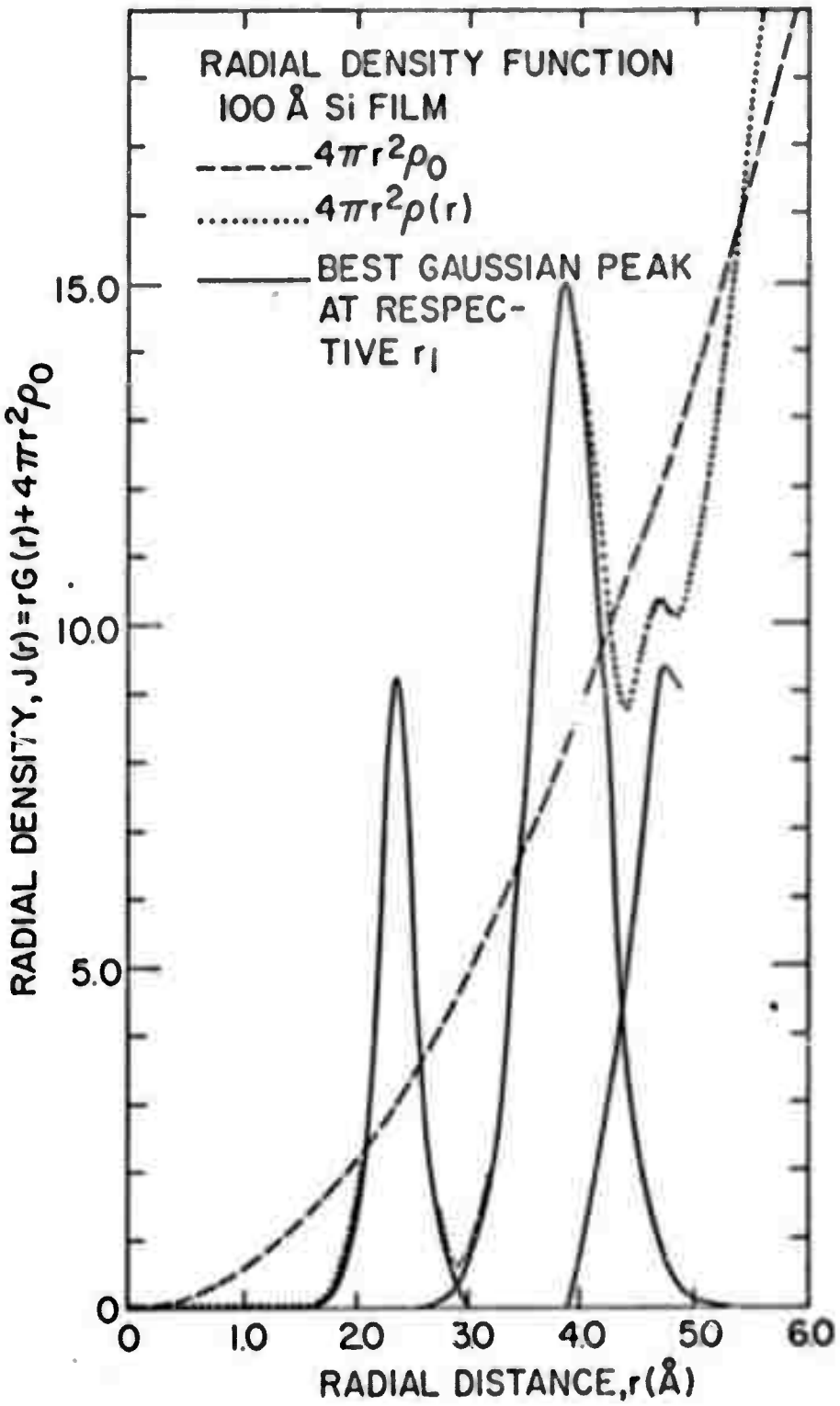
RADIAL DENSITY FUNCTION
100 Å Si FILM
$4\pi r^2\rho_0$
$4\pi r^2\rho(r)$
BEST GAUSSIAN PEAK AT RESPECTIVE r_1
RADIAL DENSITY, $J(r)=rG(r)+4\pi r^2\rho_0$
15.0
10.0
5.0
0
0
1.0
2.0
3.0
4.0
5.0
6.0
RADIAL DISTANCE, r(Å)

Fig. 10.

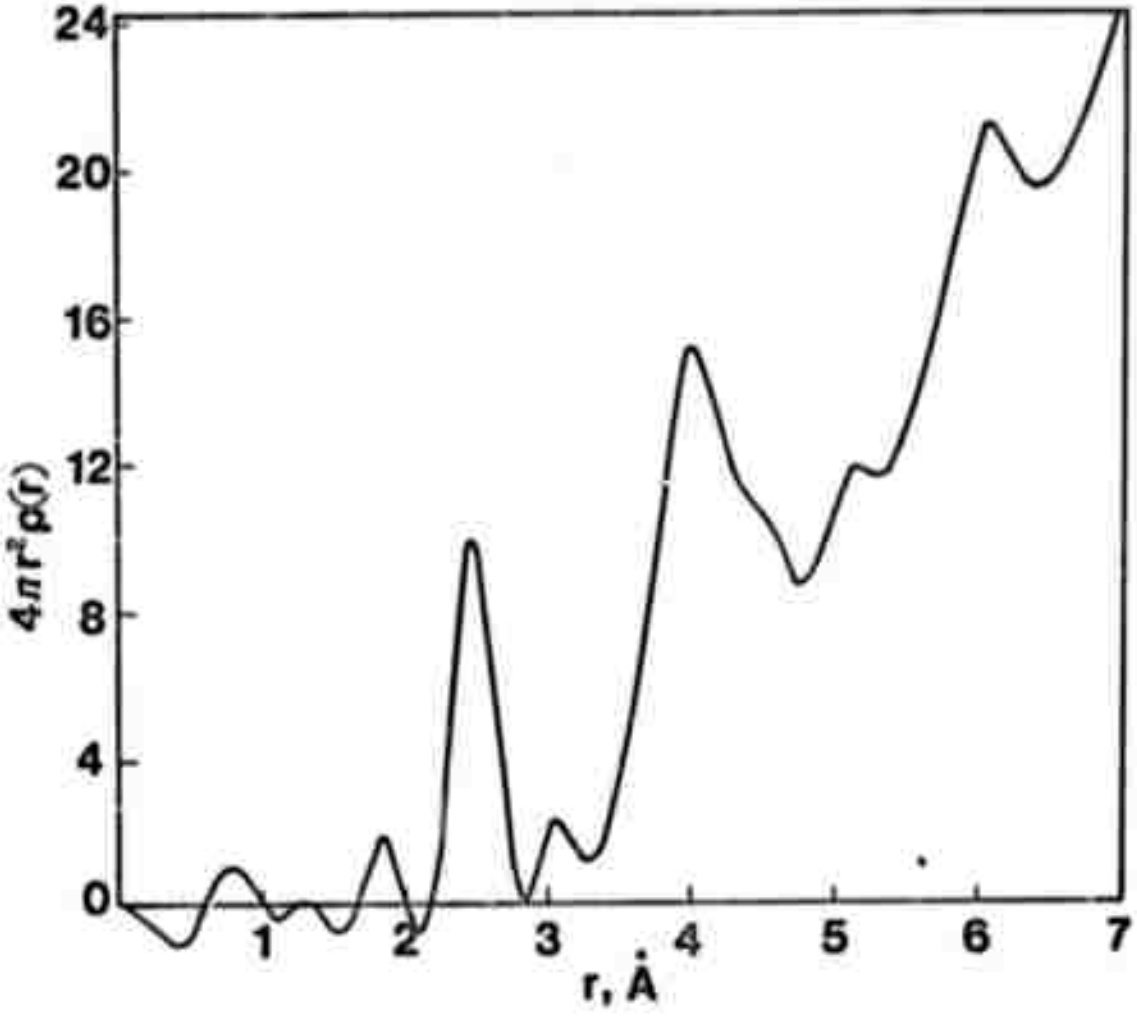

Fig. 11(a)

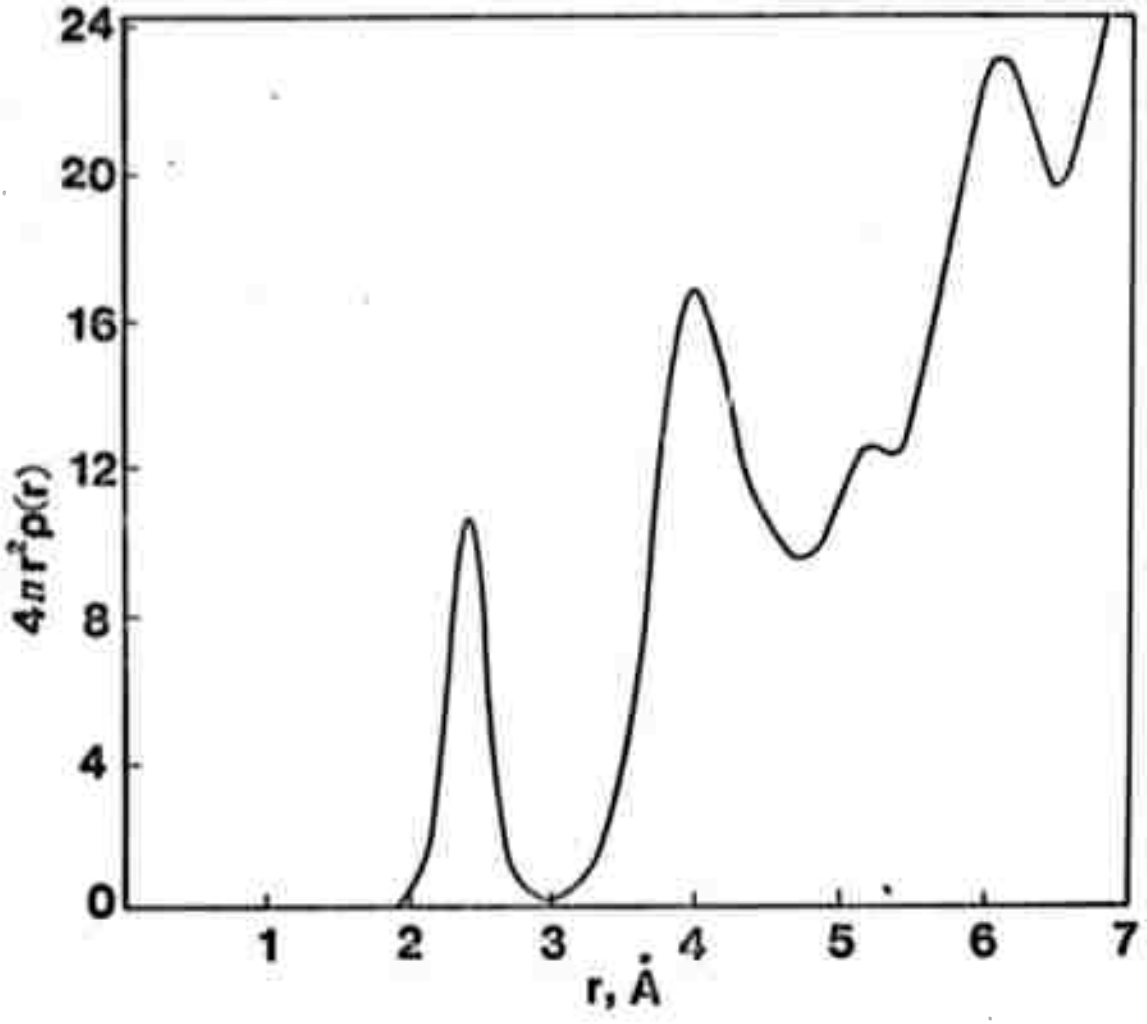

Fig. 11(b)

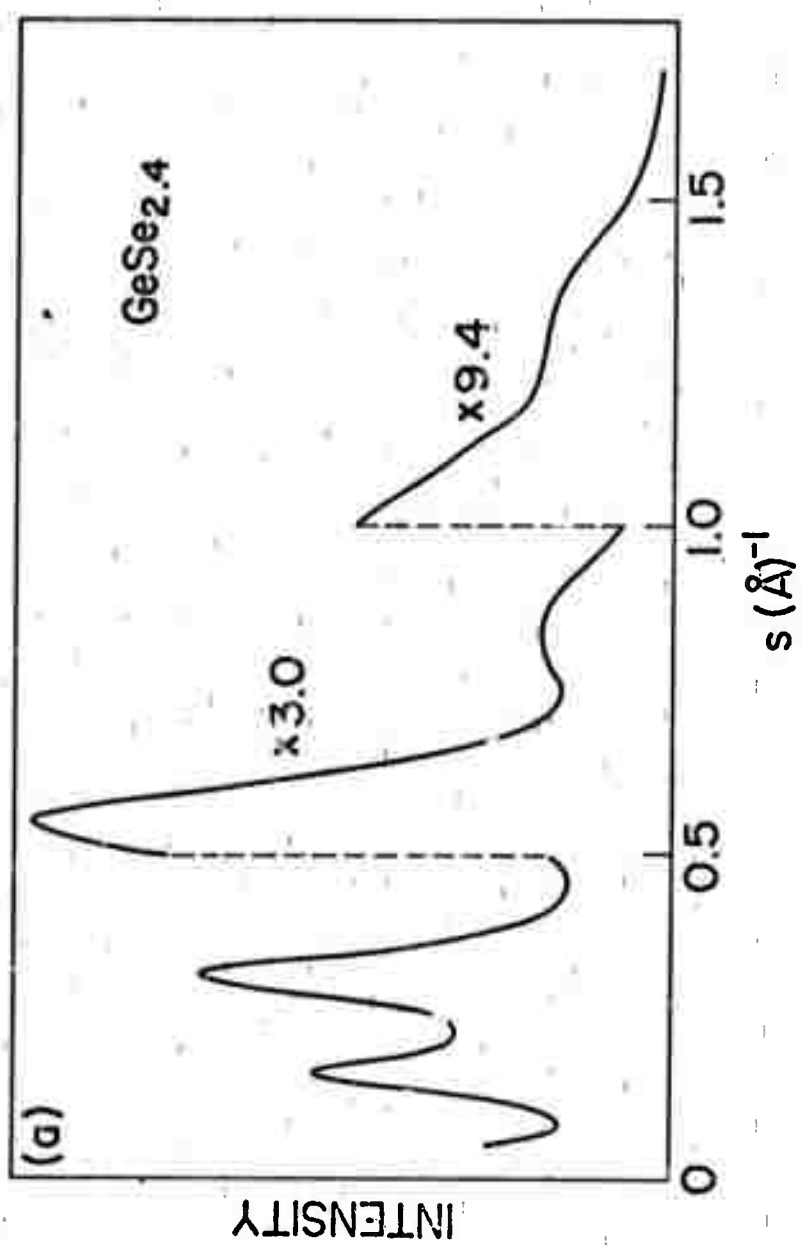

Fig. 12.

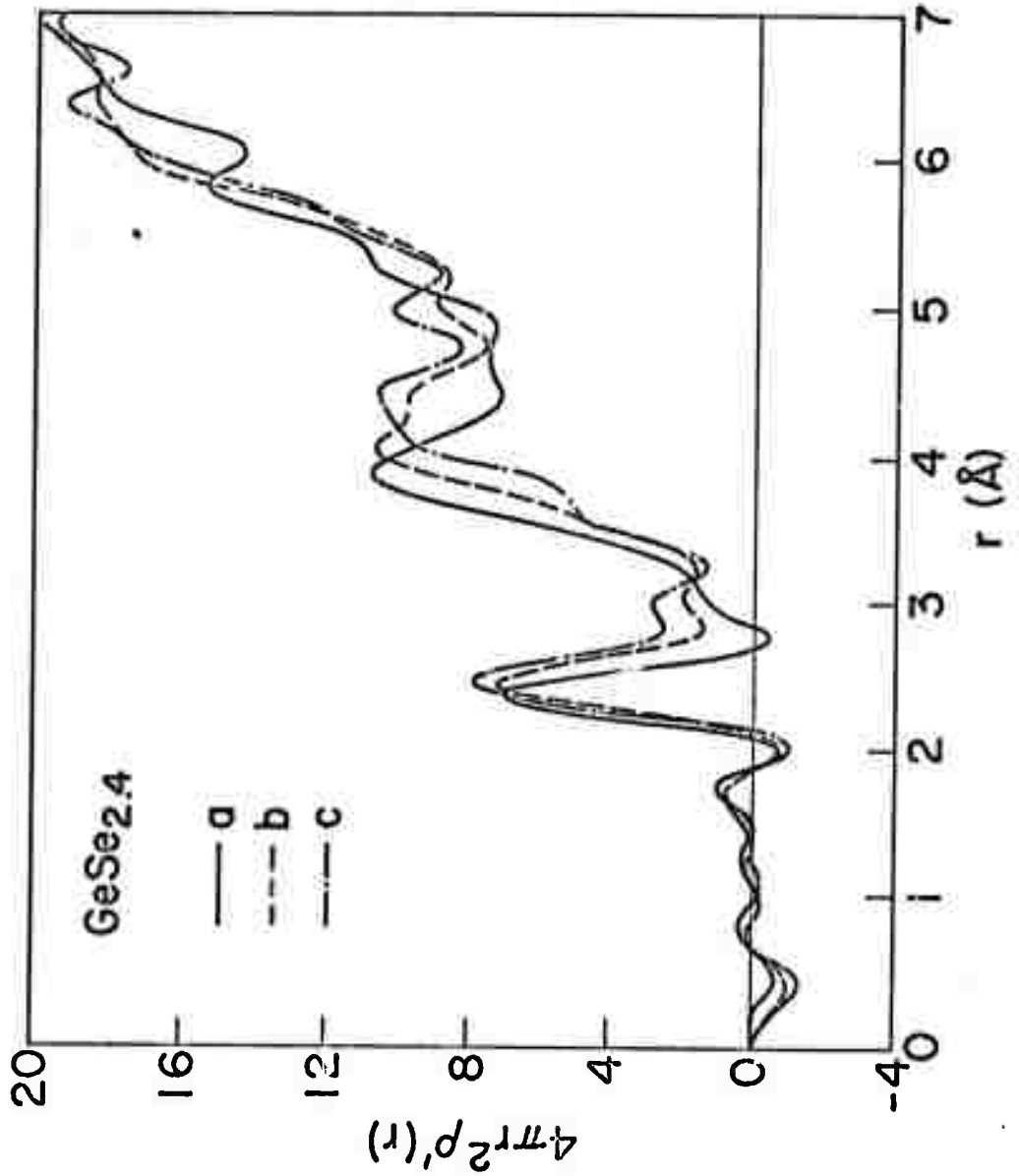

Fig. 13.

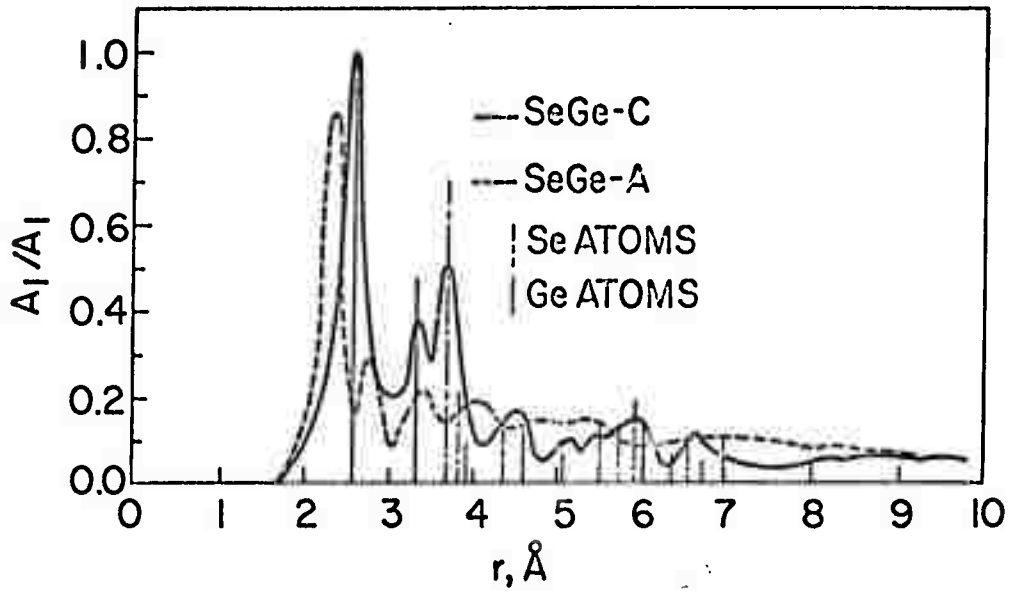
1.0
0.8
0.6
0.4
0.2
0.0
A_1/A_1
SeGe-C
SeGe-A
Se ATOMS
Ge ATOMS
0 1 2 3 4 5 6 7 8 9 10
r, Å

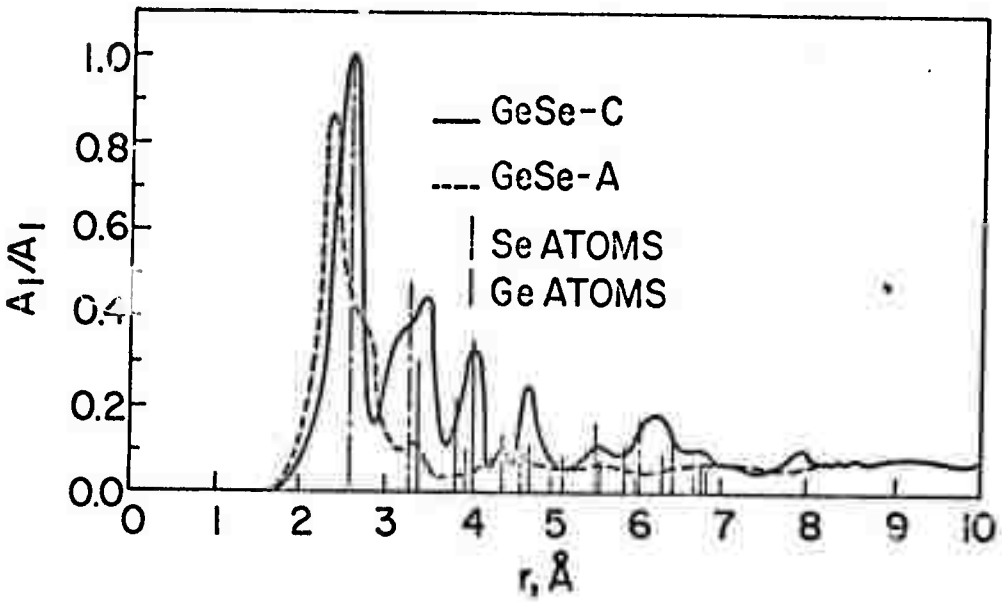
1.0
0.8
0.6
0.4
0.2
0.0
A_1/A_1
GeSe-C
GeSe-A
Se ATOMS
Ge ATOMS
0 1 2 3 4 5 6 7 8 9 10
r, Å

Fig. 14.

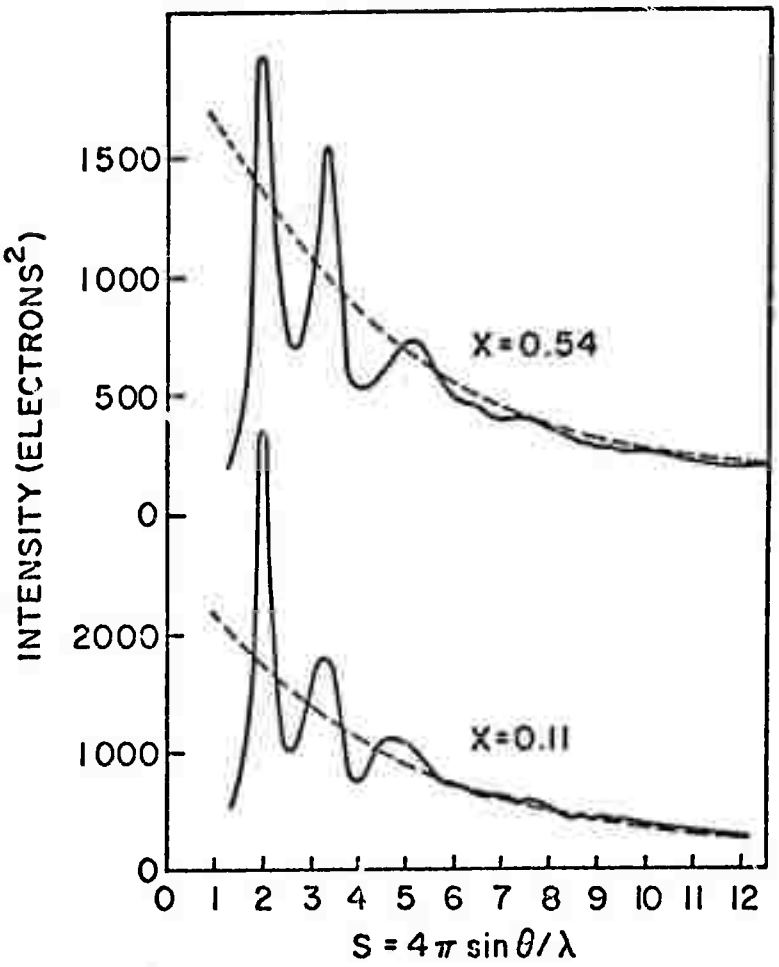
INTENSITY (ELECTRONS^2)
1500
1000
500
0
2000
1000
0
X=0.54
X=0.11
0 1 2 3 4 5 6 7 8 9 10 11 12
S = 4π sin θ/λ

Fig. 15.

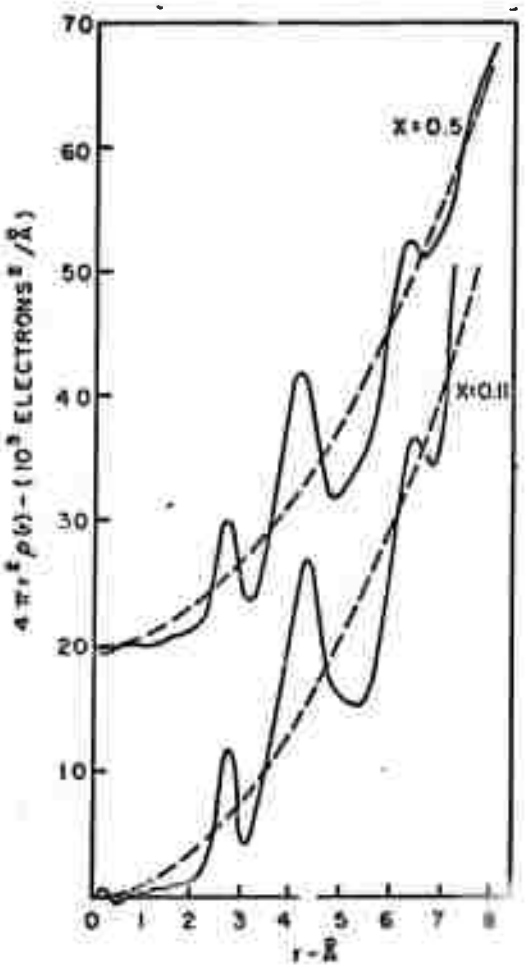
70
60
50
40
30
20
10
0
1
2
3
4
5
6
7
8
X=0.5
X=0.11
$4\pi r^2 \rho(r) - (10^3$ ELECTRONS^2 /Å^3)
r - Å

Fig. 16.